

Semileptonic and radiative decays of the B_c meson in light-front quark model

Ho-Meoyng Choi^a and Chueng-Ryong Ji^b

^a Department of Physics, Teachers College, Kyungpook National University, Daegu, Korea 702-701

^b Department of Physics, North Carolina State University, Raleigh, NC 27695-8202

We investigate the exclusive semileptonic $B_c \rightarrow (D, \eta_c, B, B_s)\ell\nu_\ell$, $\eta_b \rightarrow B_c\ell\nu_\ell$ ($\ell = e, \mu, \tau$) decays using the light-front quark model constrained by the variational principle for the QCD motivated effective Hamiltonian. The form factors $f_+(q^2)$ and $f_-(q^2)$ are obtained from the analytic continuation method in the $q^+ = 0$ frame. While the form factor $f_+(q^2)$ is free from the zero-mode, the form factor $f_-(q^2)$ is not free from the zero-mode in the $q^+ = 0$ frame. We quantify the zero-mode contributions to $f_-(q^2)$ for various semileptonic B_c decays. Using our effective method to relate the non-wave function vertex to the light-front valence wave function, we incorporate the zero-mode contribution as a convolution of zero-mode operator with the initial and final state wave functions. Our results are then compared to the available experimental data and the results from other theoretical approaches. Since the prediction on the magnetic dipole $B_c^* \rightarrow B_c + \gamma$ decay turns out to be very sensitive to the mass difference between B_c^* and B_c mesons, the decay width $\Gamma(B_c^* \rightarrow B_c\gamma)$ may help in determining the mass of B_c^* experimentally. Furthermore, we compare the results from the harmonic oscillator potential and the linear potential and identify the decay processes that are sensitive to the choice of confining potential. From the future experimental data on these sensitive processes, one may obtain more realistic information on the potential between quark and antiquark in the heavy meson system.

I. INTRODUCTION

The exclusive semileptonic decay processes of heavy mesons generated a great excitement not only in extracting the most accurate values of Cabibbo-Kobayashi-Maskawa (CKM) matrix elements but also in testing diverse theoretical approaches to describe the internal structure of hadrons. The great virtue of semileptonic decay processes is that the effects of the strong interaction can be separated from the effects of the weak interaction into a set of Lorentz-invariant form factors, i.e., the essential informations of the strongly interacting quark/gluon structure inside hadrons. Thus, the theoretical problem associated with analyzing semileptonic decay processes is essentially that of calculating the weak form factors.

In particular, along with the experimental study planned both at the Tevatron and at the Large Hadron Collider (LHC), the study of the B_c meson has been very interesting due to its outstanding feature; i.e., the B_c meson is the lowest bound state of two heavy (b, c) quarks with different flavors. Because of the fact that the B_c meson carries the flavor explicitly, not like the symmetric heavy quarkonium ($b\bar{b}$, $c\bar{c}$) states, there is no gluon or photon annihilation via strong interaction or electromagnetic interaction. It can decay only via weak interaction. Since both b - and c -quarks forming the B_c meson are heavy, the B_c meson can decay appreciably not only through the $b \rightarrow q$ ($q = c, u$) transition with c quark being a spectator but also through the $c \rightarrow q$ ($q = s, d$) transition with b quark being a spectator. The former transitions correspond to the semileptonic decays to η_c and D mesons, while the latter transitions correspond to the decays to B_s and B mesons. The latter transitions are governed typically by much larger CKM matrix element; e.g., $|V_{cs}| \sim 1$ for $B_c \rightarrow B_s\ell\nu_\ell$ ($\ell = e, \mu$), vs. $|V_{cb}| \sim 0.04$ for $B_c \rightarrow \eta_c\ell\nu_\ell$ ($\ell = e, \mu, \tau$). For this reason, although the

phase space in $c \rightarrow s, d$ transitions is much smaller than that in $b \rightarrow c, u$ transitions, the c -quark decays provide about $\sim 70\%$ to the decay width of B_c . The b -quark decays and weak annihilation add about 20% and 10%, respectively [1]. This indicates that both b - and c -quark decay processes contribute on a comparable footing to the B_c decay width.

There are many theoretical approaches to the calculation of exclusive B_c semileptonic decay modes. Although we may not be able to list them all, we may note here the following works: QCD sum rules [1, 2, 3, 4], the relativistic quark model [5, 6, 7] based on an effective Lagrangian describing the coupling of hadrons to their constituent quarks, the quasipotential approach to the relativistic quark model [8, 9, 10], the instantaneous nonrelativistic approach to the Bethe-Salpeter (BS) equation [11], the relativistic quark model based on the BS equation [12, 13], the QCD relativistic potential model [14], the relativistic quark-meson model [15], the nonrelativistic quark model [16], the covariant light-front quark model [17], and the constituent quark model [18, 19, 20, 21] using BSW (Bauer, Stech, and Wirbel) model [22] and ISGW (Isgur, Scora, Grinstein, and Wise) model [23].

The purpose of this paper is to extend our light-front quark model (LFQM) [24, 25, 26, 27, 28, 29] based on the QCD-motivated effective LF Hamiltonian to calculate the hadronic form factors and decay widths for the exclusive semileptonic $B_c \rightarrow P\ell\nu_\ell$ ($P = D, D_s, B, B_s$) and $\eta_b \rightarrow B_c\ell\nu_\ell$ decays and the magnetic dipole $B_c^* \rightarrow B_c\gamma$ transition. In our previous LFQM analysis [24, 25, 26, 27, 28, 29], we have analyzed the meson mass spectra [24, 25] and various exclusive processes of the ground state pseudoscalar (P) and vector (V) mesons such as the $P \rightarrow P$ semileptonic heavy/light meson decays [25, 26], the rare $B \rightarrow K\ell^+\ell^-$ decays [27], and the magnetic dipole transitions of the low-lying heavy/light pseu-

doscalar/vector mesons [24, 28, 29]. In those analyses, we found a good agreement with the experimental data. However, since we didn't analyze the B_c and B_c^* mesons yet, we shall extend our LFQM to predict the masses and the decay constants of B_c and B_c^* mesons as well as the above mentioned exclusive decays of B_c and B_c^* mesons.

Our LFQM [24, 25, 26, 27, 28, 29] analysis in this work has several salient features: (1) We have implemented the variational principle to the QCD motivated effective LF Hamiltonian to enable us to analyze the meson mass spectra and to find optimized model parameters. The present investigation further constrains the phenomenological parameters and extends the applicability of our LFQM to the wider range of hadronic phenomena. (2) We have performed the analytical continuation from the spacelike region to the physical timelike region to obtain the weak form factor $f_+(q^2)$ for the exclusive semileptonic decays between the two pseudoscalar mesons as well as to obtain the decay form factors $F_{VP}(q^2)$ for $V \rightarrow P\gamma^*$ transitions. The Drell-Yan-West ($q^+ = q^0 + q^3 = 0$) frame (i.e., $q^2 = -\mathbf{q}_\perp^2 < 0$) is useful because only the valence contributions are needed unless the zero-mode contribution exists.

The form factor $f_+(q^2)$ can be obtained just from the valence contribution in the $q^+ = 0$ frame without encountering the zero-mode contribution [30]. However, the form factor $f_-(q^2)$ receives the higher Fock state contribution (i.e., the zero-mode in the $q^+ = 0$ frame or the nonvalence contribution in the $q^+ > 0$ frame) within the framework of LF quantization. Thus, it is necessary to include either the zero-mode contribution (if working in the $q^+ = 0$ frame) or the nonvalence contribution (if working in the $q^+ > 0$ frame) to obtain the form factor $f_-(q^2)$. In this work, we utilize our effective method presented in [26] to express the zero-mode contribution as a convolution of zero-mode operator that we find in this work with the initial and final state LF wave functions. In this way, we calculate the form factor $f_-(q^2)$ in the $q^+ = 0$ frame with the perpendicular components of the currents and discuss the LF covariance of $f_-(q^2)$ in the valence region by analyzing the covariant BS model and the LF covariant analysis described by Jaus [31]. We also estimate the zero-mode contributions to the $f_-(q^2)$ for various semileptonic B_c decays in our LFQM.

The paper is organized as follows. In Sec. II, we discuss the $P \rightarrow P$ semileptonic decays using an exactly solvable model based on the covariant BS model of (3+1)-dimensional fermion field theory. We explicitly show the equivalence between the results obtained by the manifestly covariant method and the LF method in the $q^+ = 0$ frame. The extraction of the zero-mode contribution to $f_-(q^2)$ in the $q^+ = 0$ frame and the effective inclusion of the zero-mode in the valence region are discussed. In Sec. III, we briefly describe the formulation of our LFQM and the procedure of fixing the model parameters using the variational principle for the QCD motivated effective Hamiltonian. The masses and decay constants of the B_c^* and B_c mesons are predicted and compared with the data

as well as other theoretical model predictions. The distribution amplitudes (DAs) for the heavy-flavored mesons such as D, η_c, B, B_s, B_c and η_b are also obtained in this section. In Sec. IV, we calculate the weak form factors $f_+(q^2)$ and $f_-(q^2)$ in the $q^+ = 0$ frame using the plus and perpendicular components of the currents, respectively. The zero-mode contribution to the form factor $f_-(q^2)$ is also discussed. In Sec. V, the decay form factor $F_{B_c^* B_c}(q^2)$ for the $B_c^* \rightarrow B_c \gamma^*$ transition and the decay width for $B_c^* \rightarrow B_c \gamma$ are presented. The coupling constant $g_{B_c^* B_c}$ needed for the calculation of the decay width for $B_c^* \rightarrow B_c \gamma$ is determined in the limit $q^2 \rightarrow 0$, i.e., $g_{B_c^* B_c} = F_{B_c^* B_c}(q^2 = 0)$. For the numerical calculation of the semileptonic and radiative decays, the form factors $f_\pm(q^2)$ for the semileptonic decays and $F_{B_c^* B_c}(q^2)$ for the $B_c^* \rightarrow B_c \gamma^*$ transition are analytically continued to the timelike $q^2 > 0$ region by changing \mathbf{q}_\perp^2 to $-q^2$ in the form factor. In Sec. VI, our numerical results (i.e., the form factors and decay rates for $B_c \rightarrow (D, \eta_c, B, B_s) \ell \nu_\ell$, $\eta_b \rightarrow B_c \ell \nu_\ell$, and $B_c^* \rightarrow B_c \gamma^*$ decays) are presented and compared with the experimental data as well as other theoretical results. Summary and discussion follow in Sec. VII.

II. $P \rightarrow P$ SEMILEPTONIC DECAYS IN COVARIANT BETHE-SALPETER MODEL

A. Manifestly covariant calculation

The amplitude A for a semileptonic decay of a meson $Q_1 \bar{q}$ with the four-momentum P_1 and the mass M_1 into another meson $Q_2 \bar{q}$ with the four-momentum P_2 and the mass M_2 is given by

$$A = \frac{G_F}{\sqrt{2}} V_{Q_1 \bar{Q}_2} L_\mu H^\mu, \quad (1)$$

where G_F is the Fermi constant, $V_{Q_1 \bar{Q}_2}$ is the relevant CKM mixing matrix element, L_μ is the lepton current

$$L_\mu = \bar{u}_{\nu_\ell} \gamma_\mu (1 - \gamma^5) v_\ell, \quad (2)$$

and H^μ is the hadron current

$$H^\mu = \langle P_2, \epsilon | (V^\mu - A^\mu) | P_1 \rangle. \quad (3)$$

Here, ϵ is the polarization of the daughter meson and V^μ and A^μ are the vector and axial vector currents, respectively. If the final state is pseudoscalar, the hadron current can be decomposed as follows:

$$\begin{aligned} \langle P_2 | A^\mu | P_1 \rangle &= 0, \\ \langle P_2 | V^\mu | P_1 \rangle &= f_+(q^2) (P_1 + P_2)^\mu + f_-(q^2) q^\mu, \end{aligned} \quad (4)$$

where $q^\mu = (P_1 - P_2)^\mu$ is the four-momentum transfer to the lepton pair ($\ell \nu_\ell$) and $m_\ell^2 \leq q^2 \leq (M_1 - M_2)^2$. Sometimes it is useful to express the matrix element of the vector current in terms of $f_+(q^2)$ and $f_0(q^2)$, which

correspond to the transition amplitudes with 1^- and 0^+ spin-parity quantum numbers in the center of mass of the lepton pair, respectively. They satisfy the following relation:

$$f_0(q^2) = f_+(q^2) + \frac{q^2}{M_1^2 - M_2^2} f_-(q^2). \quad (5)$$

Including the nonzero lepton mass, the differential decay rate for the exclusive $0^- \rightarrow 0^- \ell \nu_\ell$ process is given by [32]

$$\begin{aligned} \frac{d\Gamma}{dq^2} &= \frac{G_F^2}{24\pi^3} |V_{Q_1 \bar{Q}_2}|^2 K(q^2) \left(1 - \frac{m_\ell^2}{q^2}\right)^2 \\ &\times \left\{ [K(q^2)]^2 \left(1 + \frac{m_\ell^2}{2q^2}\right) |f_+(q^2)|^2 \right. \\ &\left. + M_1^2 \left(1 - \frac{M_2^2}{M_1^2}\right)^2 \frac{3}{8} \frac{m_\ell^2}{q^2} |f_0(q^2)|^2 \right\}, \quad (6) \end{aligned}$$

where $K(q^2)$ is the kinematic factor given by

$$K(q^2) = \frac{1}{2M_1} \sqrt{(M_1^2 + M_2^2 - q^2)^2 - 4M_1^2 M_2^2}. \quad (7)$$

The solvable model, based on the covariant Bethe-Salpeter (BS) model of $(3+1)$ -dimensional fermion field theory [33, 34, 35], enables us to derive the transition form factors between two pseudoscalar mesons explicitly. The matrix element $\mathcal{M}^\mu \equiv \langle P_2 | V^\mu | P_1 \rangle$ in this BS model is given by

$$\mathcal{M}^\mu = ig_1 g_2 \Lambda_1^2 \Lambda_2^2 \int \frac{d^4 k}{(2\pi)^4} \frac{S^\mu}{N_{\Lambda_1} N_1 N_{\bar{q}} N_2 N_{\Lambda_2}}, \quad (8)$$

where g_1 and g_2 are the normalization factors which can be fixed by requiring both charge form factors of pseudoscalar mesons to be unity at zero momentum transfer, respectively. To regularize the covariant fermion triangle-loop in $(3+1)$ dimensions, we replace the point gauge-boson vertex $\gamma^\mu(1 - \gamma_5)$ by a non-local (smeared) gauge-boson vertex $(\Lambda_1^2/N_{\Lambda_1})\gamma^\mu(1 - \gamma_5)(\Lambda_2^2/N_{\Lambda_2})$, where $N_{\Lambda_1} = p_1^2 - \Lambda_1^2 + i\epsilon$ and $N_{\Lambda_2} = p_2^2 - \Lambda_2^2 + i\epsilon$, and thus the factor $(\Lambda_1 \Lambda_2)^2$ appears in the normalization factor. Λ_1 and Λ_2 play the role of momentum cut-offs similar to the Pauli-Villars regularization [33, 34]. The rest of the denominators in Eq. (8), i.e., $N_1 N_{\bar{q}} N_2$, are coming from

the intermediate fermion propagators in the triangle loop diagram and are given by

$$\begin{aligned} N_1 &= p_1^2 - m_1^2 + i\epsilon, \\ N_{\bar{q}} &= k^2 - m_{\bar{q}}^2 + i\epsilon, \\ N_2 &= p_2^2 - m_2^2 + i\epsilon, \end{aligned} \quad (9)$$

where m_1 , $m_{\bar{q}}$, and m_2 are the masses of the constituents carrying the intermediate four-momenta $p_1 = P_1 - k$, k , and $p_2 = P_2 - k$, respectively. Furthermore, the trace term in Eq. (8), S^μ , is given by

$$\begin{aligned} S^\mu &= \text{Tr}[\gamma_5(\not{p}_1 + m_1)\gamma^\mu(\not{p}_2 + m_2)\gamma_5(-\not{k} + m_{\bar{q}})] \\ &= 4(k \cdot P_2 - k^2 + m_2 m_{\bar{q}})P_1^\mu \\ &\quad + 4(k \cdot P_1 - k^2 + m_1 m_{\bar{q}})P_2^\mu \\ &\quad + 4(k^2 - P_1 \cdot P_2 - m_1 m_{\bar{q}} - m_2 m_{\bar{q}} + m_1 m_2)k^\mu. \end{aligned} \quad (10)$$

We then decompose the product of five denominators given in Eq. (8) as follows:

$$\begin{aligned} \frac{1}{N_{\Lambda_1} N_1 N_{\bar{q}} N_2 N_{\Lambda_2}} &= \frac{1}{(\Lambda_1^2 - m_1^2)(\Lambda_2^2 - m_2^2)} \\ &\quad \times \frac{1}{N_{\bar{q}}} \left(\frac{1}{N_{\Lambda_1}} - \frac{1}{N} \right) \left(\frac{1}{N_{\Lambda_2}} - \frac{1}{N} \right). \end{aligned} \quad (11)$$

Once we reduce the five propagators into a sum of terms containing three propagators using Eq. (11), we use the Feynman parametrization for the three propagators, e.g.,

$$\begin{aligned} \frac{1}{N_1 N_{\bar{q}} N_2} &= \int_0^1 dx \int_0^{1-x} dy \\ &\quad \times \frac{2}{[N_{\bar{q}} + (N_1 - N_{\bar{q}})x + (N_2 - N_{\bar{q}})y]^3}. \end{aligned} \quad (12)$$

We then make a Wick rotation of Eq. (8) in D -dimensions to regularize the integral, since otherwise one loses the logarithmically divergent terms in Eq. (8). Following the above procedure, we finally obtain the Lorentz-invariant form factors $f_+(q^2)$ and $f_-(q^2)$ as follows:

$$\begin{aligned}
f_+(q^2) &= \frac{N}{8\pi^2(\Lambda_1^2 - m_1^2)(\Lambda_2^2 - m_2^2)} \int_0^1 dx \int_0^{1-x} dy \left\{ [3(x+y) - 4] \ln \left(\frac{C_{\Lambda_1 m_2} C_{m_1 \Lambda_2}}{C_{\Lambda_1 \Lambda_2} C_{m_1 m_2}} \right) \right. \\
&\quad \left. + \left[(1-x-y)^2 (xM_1^2 + yM_2^2) + xy(2-x-y)q^2 + (x+y)(m_1 m_2 - m_1 m_{\bar{q}} - m_2 m_{\bar{q}}) + m_{\bar{q}}(m_1 + m_2) \right] C \right\}, \\
f_-(q^2) &= \frac{N}{8\pi^2(\Lambda_1^2 - m_1^2)(\Lambda_2^2 - m_2^2)} \int_0^1 dx \int_0^{1-x} dy \left\{ 3(x-y) \ln \left(\frac{C_{\Lambda_1 m_2} C_{m_1 \Lambda_2}}{C_{\Lambda_1 \Lambda_2} C_{m_1 m_2}} \right) + \left[(yM_2^2 - xM_1^2) \right. \right. \\
&\quad \left. \left. + (x^2 - y^2)(xM_1^2 + yM_2^2) - xy(x-y)q^2 + (x-y)(m_1 m_2 - m_1 m_{\bar{q}} - m_2 m_{\bar{q}}) + m_{\bar{q}}(m_2 - m_1) \right] C \right\},
\end{aligned} \tag{13}$$

where $N = g_1 g_2 \Lambda_1^2 \Lambda_2^2$ and $C = (1/C_{\Lambda_1 \Lambda_2} - 1/C_{\Lambda_1 m_2} - 1/C_{m_1 \Lambda_2} + 1/C_{m_1 m_2})$ with

$$\begin{aligned}
C_{\Lambda_1 \Lambda_2} &= (1-x-y)(xM_1^2 + yM_2^2) + xyq^2 - (x\Lambda_1^2 + y\Lambda_2^2) - (1-x-y)m_{\bar{q}}^2, \\
C_{\Lambda_1 m_2} &= (1-x-y)(xM_1^2 + yM_2^2) + xyq^2 - (x\Lambda_1^2 + ym_2^2) - (1-x-y)m_{\bar{q}}^2, \\
C_{m_1 \Lambda_2} &= (1-x-y)(xM_1^2 + yM_2^2) + xyq^2 - (xm_1^2 + y\Lambda_2^2) - (1-x-y)m_{\bar{q}}^2, \\
C_{m_1 m_2} &= (1-x-y)(xM_1^2 + yM_2^2) + xyq^2 - (xm_1^2 + ym_2^2) - (1-x-y)m_{\bar{q}}^2.
\end{aligned} \tag{14}$$

Note that the logarithmic terms in $f_+(q^2)$ and $f_-(q^2)$ are obtained from the dimensional regularization with the Wick rotation.

B. Light-front calculation

Performing the LF calculation of Eq. (8) in the $q^+ = 0$ frame in parallel with the manifestly covariant calculation, we shall use the plus and perpendicular components of the currents to obtain the form factors $f_+(q^2)$ and $f_-(q^2)$, respectively. That is, in the $q^+ = 0$ frame, one obtains the relations between the current matrix elements and the weak form factors as follows

$$\begin{aligned}
f_+(q^2) &= \frac{\mathcal{M}^+}{2P_1^+}, \\
f_-(q^2) &= f_+(q^2) + \frac{\mathcal{M}^\perp \cdot \mathbf{q}_\perp}{\mathbf{q}_\perp^2}.
\end{aligned} \tag{15}$$

The LF calculation for the trace term in Eq. (10) can be separated into the on-shell propagating part S_{on}^μ and the instantaneous part S_{inst}^μ via

$$\not{p} + m = (\not{p}_{\text{on}} + m) + \frac{1}{2} \gamma^+ (p^- - p_{\text{on}}^-) \tag{16}$$

as

$$S^\mu = S_{\text{on}}^\mu + S_{\text{inst}}^\mu, \tag{17}$$

where

$$S_{\text{on}}^\mu = 4 \left[p_{1\text{on}}^\mu (p_{2\text{on}} \cdot k_{\text{on}}) - k_{\text{on}}^\mu (p_{1\text{on}} \cdot p_{2\text{on}}) + p_{2\text{on}}^\mu (p_{1\text{on}} \cdot k_{\text{on}}) + m_2 m_{\bar{q}} p_{1\text{on}}^\mu + m_1 m_{\bar{q}} p_{2\text{on}}^\mu + m_1 m_2 k_{\text{on}}^\mu \right], \tag{18}$$

and

$$\begin{aligned}
S_{\text{inst}}^\mu &= 2(p_1^- - p_{1\text{on}}^-) \left[p_{2\text{on}}^\mu k_{\text{on}}^+ - p_{2\text{on}}^+ k_{\text{on}}^\mu + g^{\mu+} (p_{2\text{on}} \cdot k_{\text{on}} + m_2 m_{\bar{q}}) \right] \\
&\quad + 2(p_2^- - p_{2\text{on}}^-) \left[p_{1\text{on}}^\mu k_{\text{on}}^+ - p_{1\text{on}}^+ k_{\text{on}}^\mu + g^{\mu+} (p_{1\text{on}} \cdot k_{\text{on}} + m_1 m_{\bar{q}}) \right] \\
&\quad + 2(k^- - k_{\text{on}}^-) \left[p_{1\text{on}}^\mu p_{2\text{on}}^+ + p_{1\text{on}}^+ p_{2\text{on}}^\mu - g^{\mu+} (p_{1\text{on}} \cdot p_{2\text{on}} - m_1 m_2) \right] \\
&\quad + 2g^{\mu+} k_{\text{on}}^+ (p_1^- - p_{1\text{on}}^-) (p_2^- - p_{2\text{on}}^-).
\end{aligned} \tag{19}$$

Note that the subscript (on) denotes the on-mass-shell ($p^2 = m^2$) quark momentum, i.e., $p^- = p_{\text{on}}^- = (m^2 + \mathbf{p}_\perp^2)/p^+$. The traces in Eqs. (18) and (19) are then obtained as

$$\begin{aligned} S_{\text{on}}^+ &= \frac{4P_1^+}{1-x} (\mathbf{k}_\perp \cdot \mathbf{k}'_\perp + \mathcal{A}_1 \mathcal{A}_2), \\ S_{\text{inst}}^+ &= 0, \end{aligned} \quad (20)$$

for the plus component of the currents and

$$\begin{aligned} S_{\text{on}}^\perp &= \frac{-2\mathbf{k}_\perp}{x(1-x)} \left[2\mathbf{k}_\perp \cdot \mathbf{k}'_\perp + (1-x)(\mathbf{q}_\perp^2 + m_1^2 + m_2^2) + 2x^2 m_q^2 + 2x(1-x)(m_1 m_{\bar{q}} + m_2 m_{\bar{q}} - m_1 m_2) \right] \\ &\quad - \frac{2\mathbf{q}_\perp}{x(1-x)} (\mathbf{k}_\perp^2 + \mathcal{A}_1^2), \\ S_{\text{inst}}^\perp &= -2P_1^+ \left[(p_1^- - p_{1\text{on}}^-) \mathbf{k}'_\perp + (p_2^- - p_{2\text{on}}^-) \mathbf{k}_\perp + x(k^- - k_{\text{on}}^-) (2\mathbf{k}_\perp + \mathbf{q}_\perp) \right], \end{aligned} \quad (21)$$

for the perpendicular components of the currents, where $\mathbf{k}'_\perp = \mathbf{k}_\perp + (1-x)\mathbf{q}_\perp$ and $\mathcal{A}_i = (1-x)m_i + xm_{\bar{q}}$ ($i = 1, 2$).

As one can see from Eqs. (20) and (21), the perpendicular components of the currents receive instantaneous contributions while the plus component of the currents does not receive them. Especially, the absence of the instantaneous contributions to the plus current indicates that there is no zero-mode contribution to the hadronic matrix element of the plus current.

1. Valence contribution

In the valence region $0 < k^+ < P_2^+$, the pole $k^- = k_{\text{on}}^- = (\mathbf{k}_\perp^2 + m_q^2 - i\epsilon)/k^+$ (i.e., the spectator quark) is located in the lower half of the complex k^- -plane. Thus, the Cauchy integration formula for the k^- integral in Eq. (8) gives

$$\mathcal{M}_{val}^\mu = \frac{N}{16\pi^3} \int_0^1 \frac{dx}{(1-x)} \int d^2\mathbf{k}_\perp \chi_1(x, \mathbf{k}_\perp) \chi_2(x, \mathbf{k}'_\perp) S_{val}^\mu, \quad (22)$$

where $S_{val}^\mu = S_{\text{on}}^\mu + S_{\text{inst}}^\mu(k^- = k_{\text{on}}^-)$ and

$$M_0^2 = \frac{\mathbf{k}_\perp^2 + m_{\bar{q}}^2}{1-x} + \frac{\mathbf{k}_\perp^2 + m_1^2}{x}, \quad M_0'^2 = \frac{\mathbf{k}'_\perp^2 + m_{\bar{q}}^2}{1-x} + \frac{\mathbf{k}'_\perp^2 + m_2^2}{x}, \quad (23)$$

and $M_{\Lambda_1}^2 = M_0^2(m_1 \rightarrow \Lambda_1)$, $M_{\Lambda_2}^2 = M_0'^2(m_2 \rightarrow \Lambda_2)$ with $\mathbf{k}'_\perp = \mathbf{k}_\perp + (1-x)\mathbf{q}_\perp$. The LF vertex functions χ_1 and χ_2 are given by

$$\chi_1(x, \mathbf{k}_\perp) = \frac{1}{x^2(M_1^2 - M_0^2)(M_1^2 - M_{\Lambda_1}^2)}, \quad \chi_2(x, \mathbf{k}'_\perp) = \frac{1}{x^2(M_2^2 - M_0'^2)(M_2^2 - M_{\Lambda_2}^2)}. \quad (24)$$

From Eqs. (20) and (21), we obtain the valence contribution to \mathcal{M}_{val}^+ and \mathcal{M}_{val}^\perp as follows

$$\begin{aligned} \mathcal{M}_{val}^+ &= \frac{NP_1^+}{4\pi^3} \int_0^1 \frac{dx}{(1-x)^2} \int d^2\mathbf{k}_\perp \chi_1(x, \mathbf{k}_\perp) \chi_2(x, \mathbf{k}'_\perp) (\mathbf{k}_\perp \cdot \mathbf{k}'_\perp + \mathcal{A}_1 \mathcal{A}_2), \\ \mathcal{M}_{val}^\perp &= \frac{N}{16\pi^3} \int_0^1 \frac{dx}{(1-x)} \int d^2\mathbf{k}_\perp \chi_1(x, \mathbf{k}_\perp) \chi_2(x, \mathbf{k}'_\perp) S_{val}^\perp, \end{aligned} \quad (25)$$

where

$$S_{val}^\perp = -2\mathbf{k}_\perp \left[M_1^2 + M_2^2 + \mathbf{q}_\perp^2 - (m_1 - m_{\bar{q}})^2 - (m_2 - m_{\bar{q}})^2 + (m_1 - m_2)^2 \right] - 2\mathbf{q}_\perp \left[(1-x)M_1^2 + xM_0^2 - (m_1 - m_{\bar{q}})^2 \right]. \quad (26)$$

From Eqs. (15) and (25), we get the LF valence contributions to $f_+(q^2)$ and $f_-(q^2)$ as follows

$$\begin{aligned}
f_+^{val}(q^2) &= \frac{N}{8\pi^3} \int_0^1 \frac{dx}{(1-x)^2} \int d^2\mathbf{k}_\perp \chi_1(x, \mathbf{k}_\perp) \chi_2(x, \mathbf{k}'_\perp) (\mathbf{k}_\perp \cdot \mathbf{k}'_\perp + \mathcal{A}_1 \mathcal{A}_2), \\
f_-^{val}(q^2) &= \frac{N}{8\pi^3} \int_0^1 \frac{dx}{(1-x)} \int d^2\mathbf{k}_\perp \chi_1(x, \mathbf{k}_\perp) \chi_2(x, \mathbf{k}'_\perp) \\
&\quad \times \left\{ -(1-x)M_1^2 + (m_2 - m_{\bar{q}})\mathcal{A}_1 - m_{\bar{q}}(m_1 - m_{\bar{q}}) + \frac{\mathbf{k}_\perp \cdot \mathbf{q}_\perp}{q^2} [M_1^2 + M_2^2 - 2(m_1 - m_{\bar{q}})(m_2 - m_{\bar{q}})] \right\}.
\end{aligned} \tag{27}$$

We note that the form factors in Eq. (27) obtained in the spacelike region using the $q^+ = 0$ frame are analytically continued to the timelike region by changing \mathbf{q}_\perp^2 to $-q^2$ in the form factors.

2. Zero-mode contribution

In the nonvalence region $P_2^+ < k^+ < P_1^+$, the poles are at $p_1^- = p_{1\text{on}}^-(m_1) = [m_1^2 + \mathbf{k}_\perp^2 - i\epsilon]/p_1^+$ (from the struck quark propagator) and $p_1^- = p_{1\text{on}}^-(\Lambda_1) = [\Lambda_1^2 + \mathbf{k}_\perp^2 - i\epsilon]/p_1^+$ (from the smeared quark-photon vertex), which are located in the upper half of the complex k^- -plane. In order to estimate the zero-mode contribution, we define $\alpha = P_2^+/P_1^+ = 1 - q^+/P_1^+ = 1 - \beta$ and then the region $P_2^+ < k^+ < P_1^+$ corresponds to $\alpha < 1 - x < 1$ or equivalently $0 < x < \beta$. That is, the zero-mode contribution ($q^+ \rightarrow 0$) to the hadronic matrix element is obtained from the $\beta \rightarrow 0$ (i.e. $x \rightarrow 0$) limit for the integration of the longitudinal momentum x . The fact that S_{on}^+ in Eq. (20) is regular in the $x \rightarrow 0$ limit implies no zero-mode contribution to $f_+(q^2)$. However, as one can see from Eq. (21), both S_{on}^\perp and S_{inst}^\perp include the terms proportional to $1/x$ (i.e. p_1^-), which are singular as $x \rightarrow 0$. Those singular terms in the perpendicular current may be the source of zero-mode contribution to the hadronic matrix element in the nonvalence region.

When we do the Cauchy integration over k^- to obtain the LF time-ordered diagrams, we use Eq. (11) to avoid the complexity of treating double p_1^- -poles. As mentioned above, the zero-mode contribution comes from the p_i^- ($i = 1, 2$) factors in $S_{nv}^\perp = S_{\text{on}}^\perp + S_{\text{inst}}^\perp$. For instance, we define the zero-mode contribution to the $1/(N_{\bar{q}}N_{\Lambda_1}N_{\Lambda_2})$ term in Eq. (11) having $p_1^- = p_{1\text{on}}^-(\Lambda_1)$ pole as

$$[\mathcal{M}_{\Lambda_1\Lambda_2}^\perp]_{\text{Z.M.}} = iN \lim_{\beta \rightarrow 0} \int_{nv} \frac{d^4k}{(2\pi)^4} \frac{S_{nv}^\perp(p_1^- = p_{1\text{on}}^-(\Lambda_1))}{N_{\bar{q}}N_{\Lambda_1}N_{\Lambda_2}}. \tag{28}$$

The zero-mode contributions to the other three terms in Eq. (11) can be defined the same way as in Eq. (28) to give the net zero-mode contribution $\mathcal{M}_{\text{Z.M.}}^\perp = [\mathcal{M}_{\Lambda_1\Lambda_2}^\perp(p_{1\text{on}}^-(\Lambda_1))]_{\text{Z.M.}} - [\mathcal{M}_{\Lambda_1m_2}^\perp(p_{1\text{on}}^-(\Lambda_1))]_{\text{Z.M.}} - [\mathcal{M}_{m_1\Lambda_2}^\perp(p_{1\text{on}}^-(m_1))]_{\text{Z.M.}} + [\mathcal{M}_{m_1m_2}^\perp(p_{1\text{on}}^-(m_1))]_{\text{Z.M.}}$. Essentially, the nonvanishing zero-mode contributions in Eq. (28) are summarized as follows:

$$\begin{aligned}
(1) \quad Z = p_1^-, p_2^-, -k^- \text{ in } S_{nv}^\perp : \\
\lim_{\beta \rightarrow 0} \int_{nv} \frac{d^4k}{(2\pi)^4} \frac{Z}{N_{\bar{q}}N_{\Lambda_1}N_{\Lambda_2}} &= \frac{i}{16\pi^3} \int_0^1 dz \int d^2\mathbf{k}_\perp \frac{\Lambda_{1\perp}^2}{\Lambda_{1\perp}^2 [z\Lambda_{2\perp}^2 + (1-z)\Lambda_{1\perp}^2]}, \\
(2) \quad Z = p_{1\text{on}}^- \text{ in } S_{nv}^\perp : \\
\lim_{\beta \rightarrow 0} \int_{nv} \frac{d^4k}{(2\pi)^4} \frac{Z}{N_{\bar{q}}N_{\Lambda_1}N_{\Lambda_2}} &= \frac{i}{16\pi^3} \int_0^1 dz \int d^2\mathbf{k}_\perp \frac{m_{1\perp}^2}{\Lambda_{1\perp}^2 [z\Lambda_{2\perp}^2 + (1-z)\Lambda_{1\perp}^2]}, \\
(3) \quad Z = p_{2\text{on}}^- \text{ in } S_{nv}^\perp : \\
\lim_{\beta \rightarrow 0} \int_{nv} \frac{d^4k}{(2\pi)^4} \frac{Z}{N_{\bar{q}}N_{\Lambda_1}N_{\Lambda_2}} &= \frac{i}{16\pi^3} \int_0^1 dz \int d^2\mathbf{k}_\perp \frac{m_{2\perp}^2 z / (z-1)}{\Lambda_{1\perp}^2 [z\Lambda_{2\perp}^2 + (1-z)\Lambda_{1\perp}^2]},
\end{aligned} \tag{29}$$

where the variable change $x = \beta z$ was made and $m_{i\perp}^2 = m_i^2 + \mathbf{p}_{i\perp}^2$ and $\Lambda_{i\perp}^2 = \Lambda_i^2 + \mathbf{p}_{i\perp}^2$. We should note that $Z = p_{i\text{on}}^- k^+ \rightarrow p_{i\text{on}}^- P_1^+$ ($i = 1, 2$) in S_{nv}^\perp and other terms such as $Z = p_{1\text{on}}^- p_2^+$ and $p_{2\text{on}}^- p_1^+$ go to zero in the $\beta \rightarrow 0$ limit. Finally, we get the following nonvanishing zero-mode contribution to the trace term S_{nv}^\perp in Eq. (28):

$$S_{\text{Z.M.}}^\perp = \lim_{x \rightarrow 0} S_{nv}^\perp = 2p_1^-(\mathbf{p}_{1\perp} + \mathbf{p}_{2\perp}) = 2p_1^-(2\mathbf{p}_{1\perp} - \mathbf{q}_\perp), \tag{30}$$

which in fact is common to other three terms in Eq. (11). After a little manipulation, we finally get the following nonvanishing zero-mode contribution to the form factor $f_-(q^2)$ in Eq. (15) as follows

$$\begin{aligned} f_-^{\text{Z.M.}}(q^2) &= i \frac{N}{(\Lambda_1^2 - m_1^2)(\Lambda_2^2 - m_2^2)} \int \frac{d^4 k}{(2\pi)^4} \frac{S_{\text{Z.M.}}^\perp \cdot \mathbf{q}_\perp}{\mathbf{q}_\perp^2} \left(\frac{1}{N_{\bar{q}} N_{\Lambda_1} N_{\Lambda_2}} - \frac{1}{N_{\bar{q}} N_{\Lambda_1} N_2} - \frac{1}{N_{\bar{q}} N_1 N_{\Lambda_2}} + \frac{1}{N_{\bar{q}} N_1 N_2} \right) \\ &= \frac{N}{8\pi^2 (\Lambda_1^2 - m_1^2)(\Lambda_2^2 - m_2^2)} \int_0^1 dz (1-2z) \ln \left(\frac{B_{\Lambda_1 m_2} B_{m_1 \Lambda_2}}{B_{\Lambda_1 \Lambda_2} B_{m_1 m_2}} \right), \end{aligned} \quad (31)$$

where

$$\begin{aligned} B_{\Lambda_1 \Lambda_2} &= z(1-z)\mathbf{q}_\perp^2 + (1-z)\Lambda_1^2 + z\Lambda_2^2, \\ B_{\Lambda_1 m_2} &= z(1-z)\mathbf{q}_\perp^2 + (1-z)\Lambda_1^2 + zm_2^2, \\ B_{m_1 \Lambda_2} &= z(1-z)\mathbf{q}_\perp^2 + (1-z)m_1^2 + z\Lambda_2^2, \\ B_{m_1 m_2} &= z(1-z)\mathbf{q}_\perp^2 + (1-z)m_1^2 + zm_2^2. \end{aligned} \quad (32)$$

Therefore, we get the LF covariant weak form factors in the $q^+ = 0$ frame as $f_+^{\text{LFCov}}(q^2) = f_+^{\text{val}}(q^2)$ and $f_-^{\text{LFCov}}(q^2) = f_-^{\text{val}}(q^2) + f_-^{\text{Z.M.}}(q^2)$.

3. Effective inclusion of the zero-mode in the valence region

In this exactly solvable covariant BS model, we find that while the matrix element of the plus current is exactly on-mass shell physical amplitude, that of the perpendicular current is the off-mass shell amplitude. As shown in our previous work [26], we can relate the non-wave-function vertex to the ordinary valence wave function in the $q^+ > 0$ frame using the iteration of the irreducible kernel involved in the bound state equation. In the $q^+ \rightarrow 0$ frame, the nonvalence contribution in the $q^+ > 0$ frame corresponds to the zero-mode contribution in the $q^+ = 0$ frame. Thus, we can identify the zero-mode operator that is convoluted with the initial and final state valence wave functions to generate the zero-mode contribution. Our method can also be realized effectively by the method presented by Jaus [31] using the orientation of the light-front plane characterized by the invariant equation $\omega \cdot x = 0$ [36, 37], where ω is an arbitrary light-like four vector. The special case $\omega = (1, 0, 0, -1)$ corresponds to the light-front or null plane $\omega \cdot x = x^+ = 0$. While the exact on-shell amplitudes (such as \mathcal{M}^+) should not depend on the orientation of the light-front plane, the off-shell matrix elements (such as \mathcal{M}^\perp) acquire a spurious ω dependence. This problem is closely associated with the violation of rotational invariance in the computation of the matrix element of a one-body current. In order to treat the complete Lorentz structure of a hadronic matrix element the authors in [31, 36] have developed a method to identify and separate spurious contributions and to determine the physical, i.e. ω independent contributions to the hadronic form factors. Below, we summarize the result of zero-mode contribution obtained from the method by Jaus [31] and discuss the equivalence with our result of zero-mode contribution.

By adopting the ω dependent light-front covariant approach as in [31, 36], we derive the light-front covariant form of the form factor $f_-(q^2)$, which effectively includes the zero-mode contribution in the valence region. In order to do this, we first decompose the four vector p_1^μ in terms of $P = (P_1 + P_2)$, q , and ω with $\omega = (1, 0, 0, -1)$ as follows [31]

$$p_1^\mu = P^\mu A_1^{(1)} + q^\mu A_2^{(1)} + \frac{1}{\omega \cdot P} \omega^\mu C_1^{(1)}. \quad (33)$$

The coefficients in Eq. (33) are given by

$$\begin{aligned} A_1^{(1)} &= \frac{\omega \cdot p_1}{\omega \cdot P} = \frac{x}{2}, \\ A_2^{(1)} &= \frac{1}{q^2} \left(p_1 \cdot q - (q \cdot P) \frac{\omega \cdot p_1}{\omega \cdot P} \right) = \frac{x}{2} + \frac{\mathbf{k}_\perp \cdot \mathbf{q}_\perp}{q^2}, \\ C_1^{(1)} &= p_1 \cdot P - P^2 A_1^{(1)} - q \cdot P A_2^{(1)} = Z_2 - N_{\bar{q}}, \end{aligned} \quad (34)$$

where $N_{\bar{q}} = k^2 - m_{\bar{q}}^2$ and

$$Z_2 = x(M_1^2 - M_0^2) + m_1^2 - m_{\bar{q}}^2 + (1-2x)M_1^2 - [q^2 + q \cdot P] \frac{\mathbf{k}_\perp \cdot \mathbf{q}_\perp}{q^2}. \quad (35)$$

Note that only the coefficient $C_1^{(1)}$ which is combined with ω^μ depends on p_1^- (i.e. zero-mode). In this exactly solvable BS model, the zero-mode contribution from p_1^- is exactly opposite to that from $N_{\bar{q}}$, i.e.

$$\begin{aligned} I[p_1^-]_{Z.M.} &= i \int_{Z.M.} \frac{d^4 k}{(2\pi)^4} \frac{p_1^-}{N_{\Lambda_1} N_1 N_{\bar{q}} N_2 N_{\Lambda_2}} \\ &= \frac{N}{16\pi^2 (\Lambda_1^2 - m_1^2) (\Lambda_2^2 - m_2^2)} \int_0^1 dz \ln \left(\frac{B_{\Lambda_1 m_2} B_{m_1 \Lambda_2}}{B_{\Lambda_1 \Lambda_2} B_{m_1 m_2}} \right) \\ &= -I[N_{\bar{q}}]_{Z.M.}. \end{aligned} \quad (36)$$

Furthermore, the zero-mode contribution $I[N_{\bar{q}}]_{Z.M.}$ from $N_{\bar{q}}$ is exactly the same as the valence contribution $I[Z_2]_{val}$ from Z_2 , where $I[Z_2]_{val}$ is given by

$$I[N_{\bar{q}}]_{Z.M.} = I[Z_2]_{val} = \frac{1}{16\pi^3} \int_0^1 \frac{dx}{1-x} \int d^2 \mathbf{k}_\perp \chi_1(x, \mathbf{k}_\perp) \chi_2(x, \mathbf{k}'_\perp) Z_2. \quad (37)$$

From the identities in Eqs. (36) and (37), the replacement $N_{\bar{q}} \rightarrow Z_2$ (or equivalently $p_1^- \rightarrow -Z_2$) in the spurious ω dependent (i.e. the zero-mode related) term $C_1^{(1)}$ in Eq. (34) becomes covariant, i.e. free from any ω dependence. Effectively, the zero-mode contribution from p_1^- in the valence region can be given by Eq. (37). Using this, we can effectively include the zero-mode contribution from the second term $p_1^- \mathbf{q}_\perp$ in Eq. (30) in the valence region. On the other hand, since the first term $p_1^- \mathbf{p}_{1\perp}$ in Eq. (30) has a tensor structure, we need the tensor decomposition [31]

$$\begin{aligned} p_1^\mu p_1^\nu &= g^{\mu\nu} A_1^{(2)} + P^\mu P^\nu A_2^{(2)} + (P^\mu q^\nu + q^\mu P^\nu) A_3^{(2)} + q^\mu q^\nu A_4^{(2)} + \frac{1}{\omega \cdot P} (P^\mu \omega^\nu + \omega^\mu P^\nu) B_1^{(2)} \\ &\quad + \frac{1}{\omega \cdot P} (q^\mu \omega^\nu + \omega^\mu q^\nu) C_1^{(2)} + \frac{1}{(\omega \cdot P)^2} \omega^\mu \omega^\nu C_2^{(2)}, \end{aligned} \quad (38)$$

where

$$\begin{aligned} A_1^{(2)} &= -\mathbf{k}_\perp^2 - \frac{(\mathbf{k}_\perp \cdot \mathbf{q}_\perp)^2}{q^2}, \quad A_2^{(2)} = [A_1^{(1)}]^2, \quad A_3^{(2)} = A_1^{(1)} A_2^{(1)}, \quad A_4^{(2)} = [A_2^{(1)}]^2 - \frac{1}{q^2} A_1^{(2)}, \\ B_1^{(2)} &= A_1^{(1)} C_1^{(1)} - A_1^{(2)}, \quad C_1^{(2)} = A_2^{(1)} C_1^{(1)} + \frac{q \cdot P}{q^2} A_1^{(2)}, \quad C_2^{(2)} = [C_1^{(1)}]^2 + \left[P^2 - \frac{(q \cdot P)^2}{q^2} \right] A_1^{(2)}. \end{aligned} \quad (39)$$

We note that the coefficients $A_i^{(2)}$ ($i = 1, \dots, 4$) are related with $\mu, \nu = +$ or \perp components and $B_1^{(2)}$ with $(\mu, \nu) = (+, -)$. According to our power counting rules mentioned above, those terms are zero-mode free. On the other hand, the coefficients $C_1^{(2)}$ and $C_2^{(2)}$ are related with $(\mu, \nu) = (-, \perp)$ and $(-, -)$, respectively. That is, the C terms are related with the zero-mode contributions. Specifically, $C_1^{(2)}$ and $C_2^{(2)}$ are related with the zero-mode contribution to the perpendicular and minus components of the currents, respectively. The zero-mode contribution from $p_1^- \mathbf{p}_{1\perp}$ is thus related with $C_1^{(2)}$ and the effective inclusion of the zero-mode in the valence region can be achieved by setting $C_1^{(2)} = 0$. This leads to

$$A_2^{(1)} N_{\bar{q}} \rightarrow A_2^{(1)} Z_2 + \frac{q \cdot P}{q^2} A_1^{(2)} \quad \text{or} \quad p_1^- \mathbf{p}_{1\perp} \rightarrow -\mathbf{q}_\perp \left[A_2^{(1)} Z_2 + \frac{q \cdot P}{q^2} A_1^{(2)} \right]. \quad (40)$$

In summary, the zero-mode contribution from $S_{Z.M.}^\perp$ given by Eq. (30) can be expressed in terms of the zero-mode operator convoluted with the initial and final state LF vertex functions:

$$I[S^\perp]_{Z.M.} = \frac{1}{16\pi^3} \int_0^1 \frac{dx}{(1-x)} \int d^2 \mathbf{k}_\perp \chi_1(x, \mathbf{k}_\perp) \chi_2(x, \mathbf{k}'_\perp) \left\{ -4\mathbf{q}_\perp \left[A_2^{(1)} Z_2 + \frac{q \cdot P}{q^2} A_1^{(2)} \right] + 2\mathbf{q}_\perp Z_2 \right\}, \quad (41)$$

as expected from our effective method presented in our previous work [26]. Consequently, the LF covariant form of the form factor $f_-(q^2)$ is obtained as

$$\begin{aligned} f_-^{\text{LFCov}}(q^2) &= \frac{N}{8\pi^3} \int_0^1 \frac{dx}{(1-x)} \int d^2 \mathbf{k}_\perp \chi_1(x, \mathbf{k}_\perp) \chi_2(x, \mathbf{k}'_\perp) \left\{ -x(1-x) M_1^2 - \mathbf{k}_\perp^2 - m_1 m_{\bar{q}} + (m_2 - m_{\bar{q}}) A_1 \right. \\ &\quad + 2 \frac{q \cdot P}{q^2} \left[\mathbf{k}_\perp^2 + 2 \frac{(\mathbf{k}_\perp \cdot \mathbf{q}_\perp)^2}{q^2} \right] + 2 \frac{(\mathbf{k}_\perp \cdot \mathbf{q}_\perp)^2}{q^2} + \frac{\mathbf{k}_\perp \cdot \mathbf{q}_\perp}{q^2} [M_2^2 - (1-x)(q^2 + q \cdot P) + 2x M_0^2] \\ &\quad \left. - (1-2x) M_1^2 - 2(m_1 - m_{\bar{q}})(m_1 + m_2) \right\}, \end{aligned} \quad (42)$$

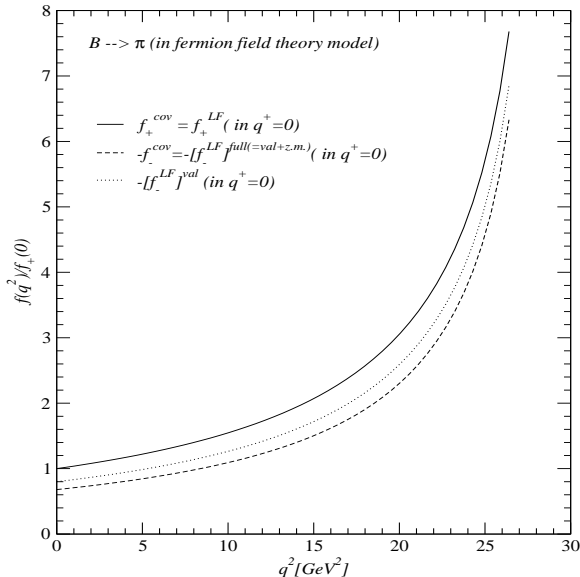


FIG. 1: The normalized weak form factors $f_{\pm}(q^2)/f_{\pm}(0)$ for $B \rightarrow \pi$ semileptonic decays obtained from the exactly solvable covariant BS model of fermion field theory.

where $q \cdot P = M_1^2 - M_2^2$.

In Fig. 1, we show our results of the normalized weak form factors $f_{\pm}(q^2)/f_{\pm}(0)$ for the semileptonic $B \rightarrow \pi$ decay obtained from the exactly solvable covariant BS model of fermion field theory. The used model parameters for B and π mesons are $M_B = 5.28$ GeV, $M_{\pi} = 0.14$ GeV, $m_b = 4.9$ GeV, $m_{u(d)} = 0.43$ GeV, $\Lambda_b = 10$ GeV, and $\Lambda_{u(d)} = 1.5$ GeV. These parameters are fixed from the normalization conditions of the π and B elastic form factors at $q^2 = 0$ [34].

The solid line represents the form factors $f_+(q^2)/f_+(0)$ obtained from the manifestly covariant result [Eq. (13)] and from the full LF calculation $f_+^{\text{LFCov}}(q^2) = f_+^{\text{val}}(q^2)$ [Eq. (27)] in the $q^+ = 0$ frame. Since the two results are in complete agreement with each other, we depict them by the single solid line. The dashed line represents the form factors $-f_-(q^2)/f_+(0)$ obtained from the manifestly covariant result [Eq. (13)] and from the full LF calculation $f_-^{\text{LFCov}}(q^2) = f_-^{\text{val}}(q^2) + f_-^{\text{Z.M.}}(q^2)$ [Eq. (42)] in the $q^+ = 0$ frame. Here again, the two results are in complete agreement with each other. The dotted line represents only the valence contribution to $-f_-(q^2)/f_+(0)$. The difference between the dashed and dotted lines amounts to the zero-mode contribution to the form factor $f_-(q^2)$.

Although our result for the $f_-^{\text{LFCov}}(q^2)$ is essentially the same as that obtained from Jaus [31], the distinguished features of our approach in deriving the LF covariant form factor may be summarized as follows: (1) We separate the trace term into the on-shell propagating part S_{on}^{μ} and the instantaneous part S_{inst}^{μ} , which enable us to classify the on-shell and off-shell matrix elements explicitly. From this one can easily find which matrix element de-

pends on the orientation of the light-front plane or equivalently receives zero-mode contributions. (2) Our power counting rule for p_1^- is very efficient method in identifying the zero-mode terms such as p_1^- and $p_1^- \mathbf{p}_{1\perp}$ that appear in the perpendicular currents and $p_1^- p_1^-$ appearing in the minus current. (3) We explicitly show that the ω dependent (i.e. zero-mode related) coefficients $C_1^{(1)}$, $C_1^{(2)}$, and $C_2^{(2)}$ correspond to p_1^- , $p_1^- \mathbf{p}_{1\perp}$ and $p_1^- p_1^-$ terms, respectively. These features in our approach should be distinguished from the approach presented in [31].

While the manifestly covariant BS model of fermion field theory model is good for the qualitative analysis of semileptonic decays, it is still semi-realistic. We thus discuss more phenomenological LFQM and the LF covariant form factors within our LFQM in the following sections.

III. MODEL DESCRIPTION

The key idea in our LFQM [24, 25] for mesons is to treat the radial wave function as a trial function for the variational principle to the QCD-motivated effective Hamiltonian saturating the Fock state expansion by the constituent quark and antiquark. The QCD-motivated Hamiltonian for a description of the ground state meson mass spectra is given by

$$\begin{aligned} H_{q\bar{q}} |\Psi_{nlm}^{JJ_z}\rangle &= \left[\sqrt{m_q^2 + \vec{k}^2} + \sqrt{m_{\bar{q}}^2 + \vec{k}^2} + V_{q\bar{q}} \right] |\Psi_{nlm}^{JJ_z}\rangle, \\ &= [H_0 + V_{q\bar{q}}] |\Psi_{nlm}^{JJ_z}\rangle = M_{q\bar{q}} |\Psi_{nlm}^{JJ_z}\rangle, \end{aligned} \quad (43)$$

where $\vec{k} = (\mathbf{k}_{\perp}, k_z)$ is the three-momentum of the constituent quark, $M_{q\bar{q}}$ is the mass of the meson, and $|\Psi_{nlm}^{JJ_z}\rangle$ is the meson wave function. In this work, we use two interaction potentials $V_{q\bar{q}}$: (1) Coulomb plus harmonic oscillator (HO) and (2) Coulomb plus linear confining potentials. The hyperfine interaction essential to distinguish pseudoscalar (0^{-+}) and vector (1^{--}) mesons is also included; viz.,

$$V_{q\bar{q}} = V_0 + V_{\text{hyp}} = a + \mathcal{V}_{\text{conf}} - \frac{4\alpha_s}{3r} + \frac{2}{3} \frac{\mathbf{S}_q \cdot \mathbf{S}_{\bar{q}}}{m_q m_{\bar{q}}} \nabla^2 V_{\text{coul}}, \quad (44)$$

where $\mathcal{V}_{\text{conf}} = br(r^2)$ for the linear (HO) potential and $\langle \mathbf{S}_q \cdot \mathbf{S}_{\bar{q}} \rangle = 1/4(-3/4)$ for the vector (pseudoscalar) meson. Using this Hamiltonian, we analyze the meson mass spectra and various wave-function-related observables, such as decay constants, electromagnetic form factors of mesons in a spacelike region, and the weak form factors for the exclusive semileptonic and rare decays of pseudoscalar mesons in the timelike region [24, 25, 26, 27, 28, 29].

The momentum-space light-front wave function of the ground state pseudoscalar and vector mesons is given by

$$\Psi_{100}^{JJ_z}(x_i, \mathbf{k}_{i\perp}, \lambda_i) = \mathcal{R}_{\lambda_1 \lambda_2}^{JJ_z}(x_i, \mathbf{k}_{i\perp}) \phi(x_i, \mathbf{k}_{i\perp}), \quad (45)$$

where $\phi(x_i, \mathbf{k}_{i\perp})$ is the radial wave function and $\mathcal{R}_{\lambda_1 \lambda_2}^{JJ_z}$ is the spin-orbit wave function that is obtained by the

interaction-independent Melosh transformation from the ordinary spin-orbit wave function assigned by the quantum numbers J^{PC} . The model wave function in Eq. (45) is represented by the Lorentz-invariant internal variables, $x_i = p_i^+/P^+$, $\mathbf{k}_{i\perp} = \mathbf{p}_{i\perp} - x_i\mathbf{P}_\perp$ and λ_i , where $P^\mu = (P^+, P^-, \mathbf{P}_\perp) = (P^0 + P^3, (M^2 + \mathbf{P}_\perp^2)/P^+, \mathbf{P}_\perp)$ is the momentum of the meson M , and p_i^μ and λ_i are the momenta and the helicities of constituent quarks, respectively.

The covariant forms of the spin-orbit wave functions for pseudoscalar and vector mesons are given by

$$\begin{aligned}\mathcal{R}_{\lambda_1\lambda_2}^{00} &= \frac{-\bar{u}_{\lambda_1}(p_1)\gamma_5 v_{\lambda_2}(p_2)}{\sqrt{2}\tilde{M}_0}, \\ \mathcal{R}_{\lambda_1\lambda_2}^{1J_z} &= \frac{-\bar{u}_{\lambda_1}(p_1)\left[\not{\epsilon}(J_z) - \frac{\epsilon \cdot (p_1 - p_2)}{M_0 + m_1 + m_2}\right]v_{\lambda_2}(p_2)}{\sqrt{2}\tilde{M}_0},\end{aligned}\quad (46)$$

where $\tilde{M}_0 = \sqrt{M_0^2 - (m_1 - m_2)^2}$, $M_0^2 = \sum_{i=1}^2(\mathbf{k}_{i\perp}^2 + m_i^2)/x_i$ is the boost invariant meson mass square obtained from the free energies of the constituents in mesons, and $\epsilon^\mu(J_z)$ is the polarization vector of the vector meson [38]. The spin-orbit wave functions satisfy the relation $\sum_{\lambda_1\lambda_2} \mathcal{R}_{\lambda_1\lambda_2}^{JJ_z\dagger} \mathcal{R}_{\lambda_1\lambda_2}^{JJ_z} = 1$ for both pseudoscalar and vector mesons. For the radial wave function ϕ , we use the same Gaussian wave function for both pseudoscalar and vector mesons:

$$\phi(x_i, \mathbf{k}_{i\perp}) = \frac{4\pi^{3/4}}{\beta^{3/2}} \sqrt{\frac{\partial k_z}{\partial x}} \exp(-\vec{k}^2/2\beta^2), \quad (47)$$

where β is the variational parameter. When the longitudinal component k_z is defined by $k_z = (x - 1/2)M_0 + (m_2^2 - m_1^2)/2M_0$, the Jacobian of the variable transformation $\{x, \mathbf{k}_\perp\} \rightarrow \vec{k} = (\mathbf{k}_\perp, k_z)$ is given by

$$\frac{\partial k_z}{\partial x} = \frac{M_0}{4x_1x_2} \left\{ 1 - \left[\frac{m_1^2 - m_2^2}{M_0^2} \right]^2 \right\}. \quad (48)$$

Note that the free kinetic part of the Hamiltonian $H_0 = \sqrt{m_q^2 + \vec{k}^2} + \sqrt{m_{q\bar{q}}^2 + \vec{k}^2}$ is equal to the free mass operator M_0 in the light-front formalism.

The normalization factor in Eq. (47) is obtained from the following normalization of the total wave function:

$$\int_0^1 dx \int \frac{d^2\mathbf{k}_\perp}{16\pi^3} |\Psi_{100}^{JJ_z}(x, \mathbf{k}_{i\perp})|^2 = 1. \quad (49)$$

We apply our variational principle to the QCD-motivated effective Hamiltonian first to evaluate the expectation value of the central Hamiltonian $H_0 + V_0$, *i.e.*, $\langle \phi | (H_0 + V_0) | \phi \rangle$ with a trial function $\phi(x_i, \mathbf{k}_{i\perp})$ that depends on the variational parameter β . Once the model parameters are fixed by minimizing the expectation value $\langle \phi | (H_0 + V_0) | \phi \rangle$, then the mass eigenvalue of each meson is obtained as $M_{q\bar{q}} = \langle \phi | (H_0 + V_{q\bar{q}}) | \phi \rangle$. Following the

above procedure, we find an analytic form of the mass eigenvalue given by

$$\begin{aligned}M_{q\bar{q}} &= \frac{1}{\beta\sqrt{\pi}} \sum_{i=q,\bar{q}} m_i^2 e^{m_i^2/2\beta^2} K_1\left(\frac{m_i^2}{2\beta^2}\right) + a\mathbf{1} \\ &+ b \left(\frac{\frac{2}{\beta\sqrt{\pi}}}{\frac{3}{2\beta^2}} \right) - \alpha_s \left[\frac{8\beta}{3\sqrt{\pi}} + \frac{32\beta^3 \langle \mathbf{S}_q \cdot \mathbf{S}_{\bar{q}} \rangle}{9m_q m_{\bar{q}} \sqrt{\pi}} \right] \mathbf{1},\end{aligned}\quad (50)$$

where $\mathbf{1} = \begin{pmatrix} 1 \\ 1 \end{pmatrix}$ and $K_1(x)$ is the modified Bessel function of the second kind. The upper and lower components of the column vector in Eq. (50) represent the results for the linear and HO potential models, respectively. Minimizing energies with respect to β and searching for a fit to the observed ground state meson spectra, our central potential V_0 obtained from our optimized potential parameters ($a = -0.72$ GeV, $b = 0.18$ GeV², and $\alpha_s = 0.31$) [24] for Coulomb plus linear potential was found to be quite comparable with the quark potential model suggested by Scora and Isgur [39] where they obtained $a = -0.81$ GeV, $b = 0.18$ GeV², and $\alpha_s = 0.3 \sim 0.6$ for the Coulomb plus linear confining potential. A more detailed procedure for determining the model parameters of light- and heavy-quark sectors can be found in our previous works [24, 25]. In this work, we obtain the new variational parameter β_{cb} for the bottom-charm sector and predict the mass eigenvalues of the low-lying B_c and B_c^* states. Our new prediction of $M_{B_c} = 6459$ [6351] MeV obtained from the linear [HO] potential model is in agreement with the data, $M_{B_c}^{\text{exp}} = (6276 \pm 4)$ MeV [40] within 3% error. We also predict the unmeasured mass of B_c^* as $M_{B_c^*} = 6494$ [6496] MeV for the linear [HO] potential model. Although it is generally believed that the linear potential is preferred between quark and antiquark in the heavy meson system, our result of the spectrum computation indicates that the HO potential is also viable and thus leads to the further investigation. We use both HO and linear potentials to compute the decay processes presented below and identify the physical observables sensitive to the choice of potential.

Our model parameters ($m_q, \beta_{q\bar{q}}$) and the predictions of the ground state meson mass spectra obtained from the linear and HO potential models are summarized in Table I and in Fig. 2, respectively, compared with the experimental data [40]. Our prediction of the η_b meson obtained from the linear [HO] potential model, $M_{\eta_b} = 9657$ [9295] MeV slightly overestimates[underestimates] the very recent data from the Babar experiment, $M_{\eta_b}^{\text{exp}} = 9388.9_{-2.3}^{+3.1}(\text{stat}) \pm 2.7(\text{syst})$ MeV [41]. Overall, however, our LFQM predictions of the ground state meson mass spectra are in agreement with the data [40] within 6% error.

The decay constants of pseudoscalar and vector mesons

TABLE I: The constituent quark mass [GeV] and the Gaussian parameters β [GeV] for the linear and HO potentials obtained by the variational principle. $q = u$ and d .

Model	m_q	m_s	m_c	m_b	β_{qq}	β_{qs}	β_{ss}	β_{qc}	β_{sc}	β_{cc}	β_{qb}	β_{sb}	β_{cb}	β_{bb}
Linear	0.22	0.45	1.8	5.2	0.3659	0.3886	0.4128	0.4679	0.5016	0.6509	0.5266	0.5712	0.8068	1.1452
HO	0.25	0.48	1.8	5.2	0.3194	0.3419	0.3681	0.4216	0.4686	0.6998	0.4960	0.5740	1.0350	1.8025

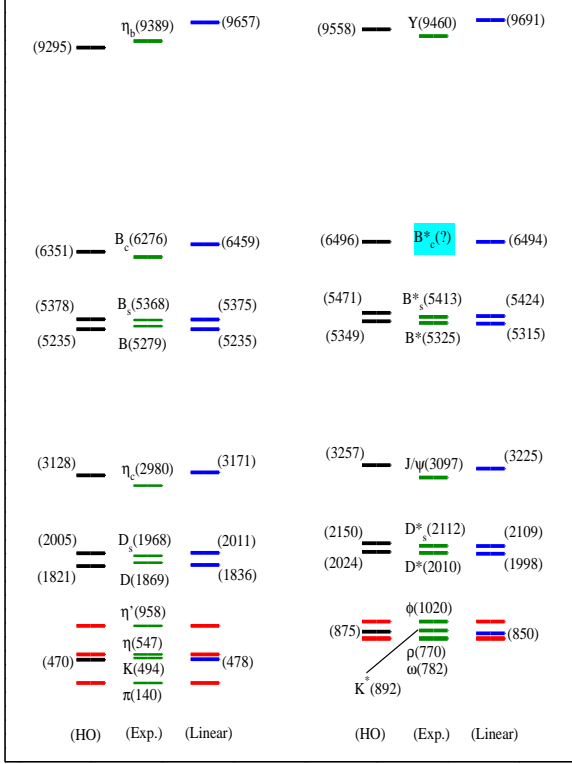


FIG. 2: (color online). Fit of the ground state meson masses[MeV] with the parameters given in Table I. The (ρ, π) , (η, η') , and (ω, ϕ) masses are our input data. The masses of $(\omega - \phi)$ and $(\eta - \eta')$ were used to determine the mixing angles of $\omega - \phi$ and $\eta - \eta'$ [24], respectively.

are defined by

$$\begin{aligned} \langle 0 | \bar{q} \gamma^\mu \gamma_5 q | P \rangle &= i f_P P^\mu, \\ \langle 0 | \bar{q} \gamma^\mu q | V(P, h) \rangle &= f_V M_V \epsilon^\mu(h). \end{aligned} \quad (51)$$

In the above definitions for the decay constants, the experimental values of pion and rho meson decay constants are $f_\pi \approx 131$ MeV from $\pi \rightarrow \mu\nu$ and $f_\rho \approx 220$ MeV from $\rho \rightarrow e^+e^-$.

Using the plus component ($\mu = +$) of the currents, one can easily calculate the decay constants. The explicit forms of pseudoscalar and vector meson decay constants

TABLE II: Bottom-charm meson decay constants(in unit of MeV) obtained from the linear [HO] parameters.

	Linear[HO]	[5]	[8]	[42]	[43]	[44]	[45]
f_{B_c}	377[508]	360	433	500	460 ± 60	517	410 ± 40
$f_{B_c^*}$	398[551]	—	503	500	460 ± 60	517	—

are given by

$$\begin{aligned} f_P &= 2\sqrt{6} \int \frac{dx d^2\mathbf{k}_\perp}{16\pi^3} \frac{\mathcal{A}}{\sqrt{\mathcal{A}^2 + \mathbf{k}_\perp^2}} \phi(x, \mathbf{k}_\perp), \\ f_V &= 2\sqrt{6} \int \frac{dx d^2\mathbf{k}_\perp}{16\pi^3} \frac{\phi(x, \mathbf{k}_\perp)}{\sqrt{\mathcal{A}^2 + \mathbf{k}_\perp^2}} \left[\mathcal{A} + \frac{2\mathbf{k}_\perp^2}{\mathcal{M}_0} \right], \end{aligned} \quad (52)$$

where $\mathcal{A} = x_2 m_1 + x_1 m_2$ and $\mathcal{M}_0 = M_0 + m_1 + m_2$. Here, only $L_z = S_z = 0$ component of the wave function contributes. We note that the vector meson decay constant f_V is extracted from the longitudinal ($h = 0$) polarization.

In Table II, we present our predictions for the decay constants of f_{B_c} and $f_{B_c^*}$ and compare with other model calculations [5, 8, 42, 43, 44, 45]. The decay constants for other light- and heavy-mesons have been predicted in our previous works [24, 28, 38] and found to be in good agreement with experimental data. While our predictions of the decay constants for the light-light and heavy-light systems [24, 28, 38] are not sensitive to the choice of potential(linear or HO), the decay constants for heavy-heavy systems such as (B_c, B_c^*) and (η_b, Υ) in [28] are quite sensitive to the choice of potential. Thus, the experimental measurements for the decay constants of (B_c, B_c^*) and (η_b, Υ) mesons may distinguish between the linear and HO potentials within our LFQM.

The process-independent quark distribution amplitude(DA) $\phi_{P(V)}(x)$ for pseudoscalar (vector) meson is the probability amplitude for finding the $q\bar{q}$ pair in the meson with $x_q = x$ and $x_{\bar{q}} = 1 - x$. It is directly related to our LF valence wave function [38]:

$$\phi_{P(V)} = \int \frac{d^2\mathbf{k}_\perp}{16\pi^3} \Psi(x, \mathbf{k}_\perp). \quad (53)$$

The \mathbf{k}_\perp integration in Eq. (53) is cut off by the ultraviolet cutoff Λ implicit in the wave function. The dependence on the scale Λ is then given by the QCD evolution equation [46] and can be calculated perturbatively. However, the DAs at a certain low scale can be obtained by the necessary nonperturbative input from LFQM. Moreover, the presence of the damping Gaussian factor in our LFQM allows us to perform the integral up to infinity without

loss of accuracy. The quark DAs for pseudoscalar and vector mesons are constrained by

$$\int_0^1 \phi_{P(V)}(x) dx = \frac{f_{P(V)}}{2\sqrt{6}}. \quad (54)$$

We show in Fig. 3 the normalized quark DAs $\Phi(x) = (2\sqrt{6}/f_P)\phi(x)$ for D (dotted line), B (dashed line), B_s (dot-dashed line), and B_c (solid line) mesons obtained from the linear (upper panel) and HO (lower panel) potential parameters, respectively. In Fig. 4, we also show the normalized quark DAs for η_c (thin lines) and η_b (thick lines) mesons obtained from the linear (solid lines) and HO (dashed lines) potential parameters. While the two model predictions for the heavy-light systems such as (D , B , and B_s) are not much different from each other, the HO potential model predictions for the heavy-heavy systems such as (η_c , B_c and η_b) give somewhat broader shapes than the linear potential model predictions.

IV. SEMILEPTONIC DECAYS OF THE B_c MESON

The relevant quark momentum variables for $P(q_1\bar{q}) \rightarrow P(q_2\bar{q}')$ transitions in the $q^+ = 0$ frames are given by

$$\begin{aligned} p_1^+ &= x_1 P_1^+, & p_{\bar{q}}^+ &= x_2 P_1^+, & \mathbf{p}_{1\perp} &= x_1 \mathbf{P}_{1\perp} - \mathbf{k}_\perp, \\ p_2^+ &= x_1 P_1^+, & p_{\bar{q}'}^+ &= x_2 P_1^+, & \mathbf{p}_{2\perp} &= x_1 \mathbf{P}_{2\perp} - \mathbf{k}'_\perp, \\ \mathbf{p}_{\bar{q}\perp} &= x_2 \mathbf{P}_{1\perp} + \mathbf{k}_\perp, & \mathbf{p}_{\bar{q}'\perp} &= x_2 \mathbf{P}_{2\perp} + \mathbf{k}'_\perp, \end{aligned} \quad (55)$$

where $x_1 = x$ and $x_2 = 1-x$ and spectator quark requires that $p_{\bar{q}}^+ = p_{\bar{q}'}^+$ and $\mathbf{p}_{\bar{q}\perp} = \mathbf{p}_{\bar{q}'\perp}$. Taking a Lorentz frame where $\mathbf{P}_{1\perp} = 0$ and $\mathbf{P}_{2\perp} = -\mathbf{q}_\perp$ amounts to $\mathbf{k}'_\perp = \mathbf{k}_\perp + (1-x)\mathbf{q}_\perp$.

The hadronic matrix element of the plus current $\mathcal{M}^+ \equiv \langle P_2 | V^+ | P_1 \rangle$ in Eq. (4) is then obtained by the convolution formula of the initial and final state LF wave functions in the valence region:

$$\begin{aligned} \mathcal{M}^+ &= \int_0^1 dx \int \frac{d^2\mathbf{k}_\perp}{16\pi^3} \phi_2(x, \mathbf{k}'_\perp) \phi_1(x, \mathbf{k}_\perp) \\ &\times \sum_{\lambda_1, \lambda_2, \bar{\lambda}} \mathcal{R}_{\lambda_2 \bar{\lambda}}^{00\dagger} \frac{\bar{u}_{\lambda_2}(p_2)}{\sqrt{p_2^+}} \gamma^+ \frac{u_{\lambda_1}(p_1)}{\sqrt{p_1^+}} \mathcal{R}_{\lambda_1 \bar{\lambda}}^{00}. \end{aligned} \quad (56)$$

Substituting the covariant form of the spin-orbit wave function for pseudoscalar meson given by Eq. (46) into Eq. (56) yields

$$\begin{aligned} \mathcal{M}^+ &= - \int_0^1 dx \int \frac{d^2\mathbf{k}_\perp}{16\pi^3} \frac{\phi_2(x, \mathbf{k}'_\perp) \phi_1(x, \mathbf{k}_\perp)}{2xP_1^+ \tilde{M}_0 \tilde{M}'_0} \\ &\times \text{Tr}[\gamma^5 (\not{p}_2 + m_2) \gamma^+ (\not{p}_1 + m_1) \gamma^5 (\not{p}_{\bar{q}} - m_{\bar{q}})], \end{aligned} \quad (57)$$

where

$$\begin{aligned} \tilde{M}_0 &= \sqrt{M_0^2 - (m_1 - m_2^2)^2} = \sqrt{\frac{\mathbf{k}_\perp^2 + \mathcal{A}_1^2}{x(1-x)}}, \\ \tilde{M}'_0 &= \sqrt{M_0'^2 - (m_2 - m_{\bar{q}}^2)^2} = \sqrt{\frac{\mathbf{k}'_\perp{}^2 + \mathcal{A}_2^2}{x(1-x)}}, \end{aligned} \quad (58)$$

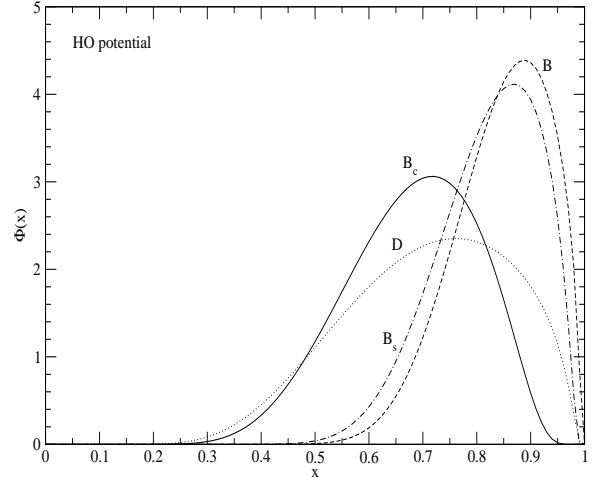
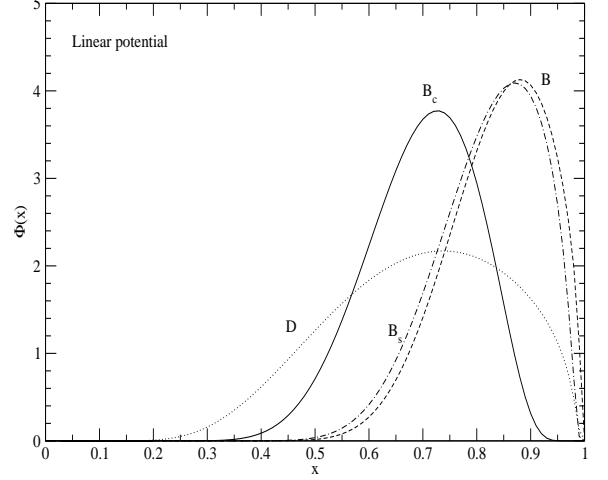


FIG. 3: The normalized distribution amplitudes for D , B , B_s , and B_c mesons obtained from the linear (upper panel) and HO (lower panel) potential parameters.

and $\mathcal{A}_i = (1-x)m_i + xm_{\bar{q}}$ ($i = 1, 2$). After some manipulation, the trace term in Eq. (57) is reduced to

$$\begin{aligned} &\text{Tr}[\gamma^5 (\not{p}_2 + m_2) \gamma^+ (\not{p}_1 + m_1) \gamma^5 (\not{p}_{\bar{q}} - m)] \\ &= - \frac{4P_1^+}{(1-x)} (\mathbf{k}_\perp \cdot \mathbf{k}'_\perp + \mathcal{A}_1 \mathcal{A}_2). \end{aligned} \quad (59)$$

Finally, the form factor $f_+(q^2)$ obtained from the valence contribution in the $q^+ = 0$ frame is given by

$$\begin{aligned} f_+(q^2) &= \int_0^1 dx \int \frac{d^2\mathbf{k}_\perp}{16\pi^3} \frac{\phi_1(x, \mathbf{k}_\perp)}{\sqrt{\mathcal{A}_1^2 + \mathbf{k}_\perp^2}} \frac{\phi_2(x, \mathbf{k}'_\perp)}{\sqrt{\mathcal{A}_2^2 + \mathbf{k}'_\perp{}^2}} \\ &\times (\mathcal{A}_1 \mathcal{A}_2 + \mathbf{k}_\perp \cdot \mathbf{k}'_\perp). \end{aligned} \quad (60)$$

We should note in the trace calculation of Eq. (59) that

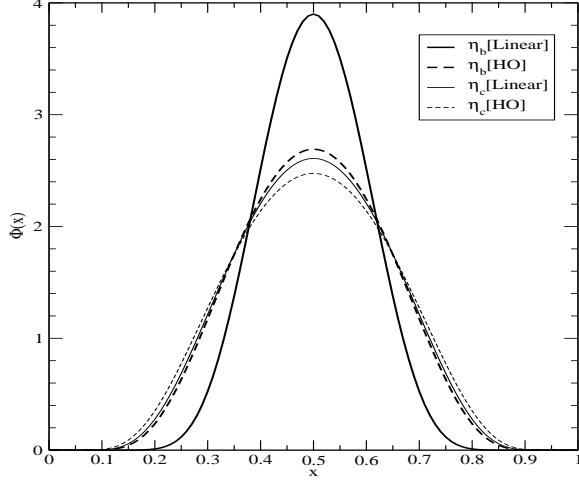


FIG. 4: The normalized distribution amplitudes for η_c (thin lines) and η_b (thick lines) mesons obtained from the linear (solid lines) and HO (dashed lines) potential parameters.

the internal momenta of the valence quarks carried inside mesons are all on-mass-shell ($p_i^2 = m_i^2$). Nevertheless, the LF valence contribution to the form factor $f_+(q^2)$ is shown to be equivalent to the covariant result as shown in Sec. II.

Comparing the manifestly covariant form factor $f_+(q^2)$ in Eq. (27) and our LFQM result $f_+(q^2)$ in Eq. (60), we find the following relations for the LF vertex functions between the two models:

$$\begin{aligned} \sqrt{2N} \frac{\chi_1(x, \mathbf{k}_\perp)}{1-x} &= \frac{\phi_1(x, \mathbf{k}_\perp)}{\sqrt{\mathcal{A}_1^2 + \mathbf{k}_\perp^2}}, \\ \sqrt{2N} \frac{\chi_2(x, \mathbf{k}'_\perp)}{1-x} &= \frac{\phi_2(x, \mathbf{k}'_\perp)}{\sqrt{\mathcal{A}_2^2 + \mathbf{k}'_\perp{}^2}}. \end{aligned} \quad (61)$$

We should note that the zero-mode operator included in Eq. (42) is independent from the choice of radial wave function.

Applying the relation in Eq. (61) to Eqs. (27) and (42), we get the following LF valence contribution $f_-^{val}(q^2)$ and the LF covariant solution $f_-^{full}(q^2)$ including both the valence and the zero-mode contributions within our LFQM:

$$\begin{aligned} f_-^{val}(q^2) &= \int_0^1 (1-x) dx \int \frac{d^2 \mathbf{k}_\perp}{16\pi^3} \frac{\phi_1(x, \mathbf{k}_\perp)}{\sqrt{\mathcal{A}_1^2 + \mathbf{k}_\perp^2}} \frac{\phi_2(x, \mathbf{k}'_\perp)}{\sqrt{\mathcal{A}_2^2 + \mathbf{k}'_\perp{}^2}} \left\{ -(1-x)M_1^2 + (m_2 - m_{\bar{q}})\mathcal{A}_1 - m_{\bar{q}}(m_1 - m_{\bar{q}}) \right. \\ &\quad \left. + \frac{\mathbf{k}_\perp \cdot \mathbf{q}_\perp}{q^2} [M_1^2 + M_2^2 - 2(m_1 - m_{\bar{q}})(m_2 - m_{\bar{q}})] \right\}, \\ f_-^{full}(q^2) &= \int_0^1 (1-x) dx \int \frac{d^2 \mathbf{k}_\perp}{16\pi^3} \frac{\phi_1(x, \mathbf{k}_\perp)}{\sqrt{\mathcal{A}_1^2 + \mathbf{k}_\perp^2}} \frac{\phi_2(x, \mathbf{k}'_\perp)}{\sqrt{\mathcal{A}_2^2 + \mathbf{k}'_\perp{}^2}} \left\{ -x(1-x)M_1^2 - \mathbf{k}_\perp^2 - m_1 m_{\bar{q}} + (m_2 - m_{\bar{q}})\mathcal{A}_1 \right. \\ &\quad \left. + 2 \frac{q \cdot P}{q^2} \left[\mathbf{k}_\perp^2 + 2 \frac{(\mathbf{k}_\perp \cdot \mathbf{q}_\perp)^2}{q^2} \right] + 2 \frac{(\mathbf{k}_\perp \cdot \mathbf{q}_\perp)^2}{q^2} + \frac{\mathbf{k}_\perp \cdot \mathbf{q}_\perp}{q^2} [M_2^2 - (1-x)(q^2 + q \cdot P) + 2xM_0^2 \right. \right. \\ &\quad \left. \left. - (1-2x)M_1^2 - 2(m_1 - m_{\bar{q}})(m_1 + m_2) \right] \right\}, \end{aligned} \quad (62)$$

where M_1 and M_2 are the physical masses of the initial and final mesons, respectively.

V. RADIATIVE $B_c^* \rightarrow B_c \gamma$ DECAY

In addition to semileptonic decays, the radiative decays of vector mesons can be analyzed within our LFQM [24, 28]. In this work, we thus calculate the decay rate for $B_c^* \rightarrow B_c \gamma$ transition.

In our LFQM calculation of $B_c^* \rightarrow B_c \gamma$ process, we first analyze the virtual photon (γ^*) decay process, calculating the momentum dependent transition form factor, $F_{B_c^* B_c}(q^2)$. The lowest-order Feynman diagram for $V \rightarrow P \gamma^*$ process is shown in Fig. 5 where the decay from

vector meson to pseudoscalar meson and virtual photon state is mediated by a quark loop with flavors of constituent mass m_1 and $m_{\bar{q}}$.

The transition form factor $F_{B_c^* B_c}(q^2)$ for $V(P_1) \rightarrow P(P_2) + \gamma^*(q)$ is defined as [28]

$$\langle P(P_2) | V^\mu | V(P_1, h) \rangle = i e \epsilon^{\mu\nu\rho\sigma} \epsilon_\nu(P_1, h) q_\rho P_{1\sigma} F_{VP}(q^2), \quad (63)$$

where the antisymmetric tensor $\epsilon^{\mu\nu\rho\sigma}$ assures electromagnetic gauge invariance, $q = P_1 - P_2$ is the four-momentum of the virtual photon, and $\epsilon_\nu(P_1, h)$ is the polarization vector of the initial meson with the four-momentum P_1 and the helicity h . The kinematically allowed q^2 (momentum transfer squared) ranges from 0 to $q_{\max}^2 = (M_V - M_P)^2$. The decay form factor $F_{B_c^* B_c}(q^2)$

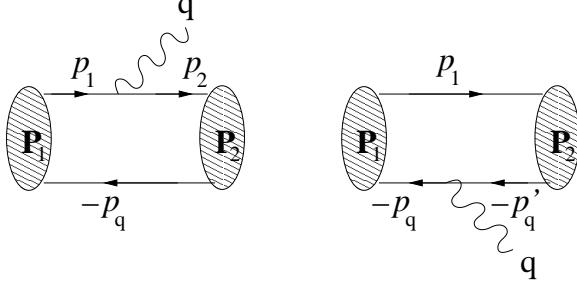


FIG. 5: The lowest order Feynman diagram for $V \rightarrow P\gamma^*$ process.

can also be obtained in the $q^+ = 0$ frame with the transverse ($h = \pm 1$) polarization and the “+”-component of the currents without encountering zero-mode contributions [30] and then analytically continued from the space-like region where the form factor is given by $F_{B_c^* B_c}(\mathbf{q}_\perp^2)$ to the timelike $q^2 > 0$ region by changing \mathbf{q}_\perp^2 to $-q^2$ in the form factor.

The hadronic matrix element of the plus current $\mathcal{M}_{VP}^+ \equiv \langle P(P_2) | V^+ | V(P_1, h) \rangle$ in Eq. (63) is then obtained by the convolution formula of the initial and final state LF wave functions in the valence region:

$$\begin{aligned} \mathcal{M}_{VP}^+ &= \sum_j e e_j \int_0^1 dx \int \frac{d^2 \mathbf{k}_\perp}{16\pi^3} \phi_2(x, \mathbf{k}_\perp) \phi_1(x, \mathbf{k}_\perp) \\ &\times \sum_{\lambda_1, \lambda_2, \bar{\lambda}} \mathcal{R}_{\lambda_2 \bar{\lambda}}^{00\ddagger} \frac{\bar{u}_{\lambda_2}(p_2)}{\sqrt{p_2^+}} \gamma^+ \frac{u_{\lambda_1}(p_1)}{\sqrt{p_1^+}} \mathcal{R}_{\lambda_1 \bar{\lambda}}^{11}, \end{aligned} \quad (64)$$

where $e e_j$ is the electrical charge for j th quark flavor. Substituting the covariant forms of the spin-orbit wave functions for pseudoscalar and vector mesons given by Eq. (46) into Eq. (64) and comparing it with the right-hand side of Eq. (63), i.e. $e P_1^+ F_{VP}(q^2) q^R / \sqrt{2}$ where $q^R = q_x + i q_y$, we could extract the one-loop integral, $I(m_1, m_{\bar{q}}, q^2)$, given by

$$\begin{aligned} I(m_1, m_{\bar{q}}, q^2) &= \int_0^1 dx \int \frac{d^2 \mathbf{k}_\perp}{8\pi^3} \frac{\phi_1(x, \mathbf{k}_\perp)}{\sqrt{\mathcal{A}_1^2 + \mathbf{k}_\perp^2}} \frac{\phi_2(x, \mathbf{k}_\perp)}{\sqrt{\mathcal{A}_1^2 + \mathbf{k}_\perp^2}} \\ &\times (1-x) \left\{ \mathcal{A}_1 + \frac{2}{\mathcal{M}_0} \left[\mathbf{k}_\perp^2 + \frac{(\mathbf{k}_\perp \cdot \mathbf{q}_\perp)^2}{q^2} \right] \right\}, \end{aligned} \quad (65)$$

where $\mathcal{M}_0 = M_0 + m_1 + m_{\bar{q}}$. The decay form factor $F_{B_c^* B_c}(q^2)$ is then obtained as [28]

$$F_{B_c^* B_c}(q^2) = e_1 I(m_1, m_{\bar{q}}, q^2) + e_2 I(m_{\bar{q}}, m_1, q^2). \quad (66)$$

The coupling constant $g_{B_c^* B_c \gamma}$ for real photon (γ) case can then be determined in the limit $q^2 \rightarrow 0$, i.e., $g_{B_c^* B_c \gamma} = F_{B_c^* B_c}(q^2 = 0)$. The decay width for $V \rightarrow P\gamma$ is given by

$$\Gamma(B_c^* \rightarrow B_c \gamma) = \frac{\alpha}{3} g_{B_c^* B_c \gamma}^2 k_\gamma^3, \quad (67)$$

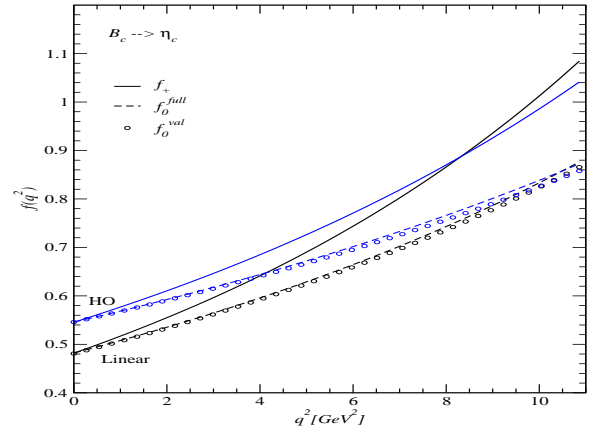
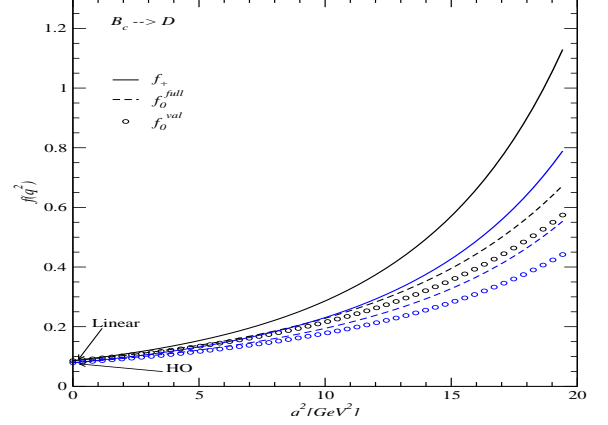


FIG. 6: (color online). The weak form factors $f_+(q^2)$ (solid line) and $f_0(q^2)$ (dashed line) for $B_c \rightarrow D$ (upper panel) and $B_c \rightarrow \eta_c$ (lower panel) semileptonic decays obtained from the linear (black line) and HO (blue line) potential parameters. The circles represent the valence contributions $f_0^{val}(q^2)$ to $f_0(q^2)$.

where α is the fine-structure constant and $k_\gamma = (M_{B_c^*}^2 - M_{B_c}^2)/2M_{B_c^*}$ is the kinematically allowed energy of the outgoing photon.

VI. NUMERICAL RESULTS

In our numerical calculations of exclusive B_c decays, we use two sets of model parameters (m, β) for the linear and HO confining potentials given in Table I obtained from the calculation of the mass spectra. Although our predictions of ground state heavy meson masses are overall in good agreement with the experimental values, we use the experimental meson masses [40] in the computations of the decay widths to reduce possible theoretical uncertainties. We also use the central values of the CKM

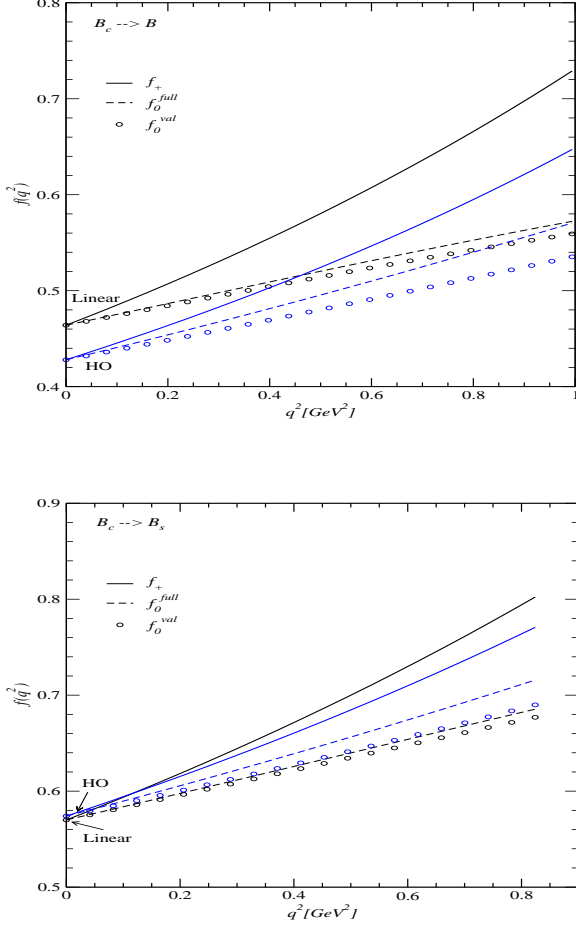


FIG. 7: (color online). The weak form factors $f_+(q^2)$ and $f_0(q^2)$ for $B_c \rightarrow B$ (upper panel) and $B_c \rightarrow B_s$ (lower panel) semileptonic decays obtained from the linear and HO potential parameters. The same line codes are used as in Fig. 6.

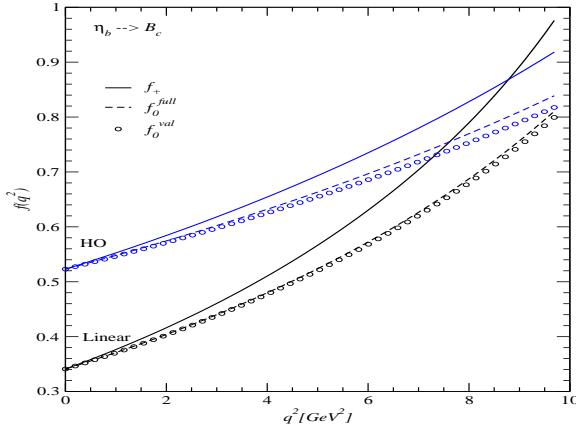


FIG. 8: (color online). The weak form factors $f_+(q^2)$ and $f_0(q^2)$ for $\eta_b \rightarrow B_c$ semileptonic decay obtained from the linear and HO potential parameters. The same line codes are used as in Fig. 6.

matrix elements,

$$\begin{aligned} |V_{ub}| &= 0.00393, & |V_{cb}| &= 0.0412, \\ |V_{cd}| &= 0.230, & |V_{cs}| &= 1.04, \end{aligned} \quad (68)$$

quoted by the Particle Data Group (PDG) [40].

In Figs. 6 and 7 we show the q^2 -dependence of the LF covariant weak form factors $f_+(q^2)$ (solid lines) and $f_0(q^2)$ (dashed lines) in the whole kinematical ranges for the CKM-suppressed (enhanced) semileptonic $B_c \rightarrow D(\eta_c)$ (Fig. 6) and $B_c \rightarrow B(B_s)$ (Fig. 7) decays obtained from both linear (black lines) and HO (blue lines) potential models. The circles represent the valence contributions $f_0^{val}(q^2)$ to $f_0(q^2)$. That is, the difference between $f_0(q^2)$ and $f_0^{val}(q^2)$ represents the zero-mode contribution to $f_0(q^2)$.

The kinematical ranges for $B_c \rightarrow D(\eta_c)$ decays induced by $b \rightarrow u(c)$ transitions with the c quark being a spectator are considerably broader than those for $B_c \rightarrow B(B_s)$ decays induced by $c \rightarrow d(s)$ transitions with the b quark being a spectator. The form factors $f_+(q^2)$ and $f_0(q^2)$ at the zero-recoil point (i.e., $q^2 = q_{\max}^2$) correspond to the overlap integral of the initial and final state meson wave functions. The maximum-recoil point (i.e., $q^2 = 0$) corresponds to a final state meson recoiling with the maximum three-momentum $|\vec{P}_f| = (M_{B_c}^2 - M_f^2)/2M_{B_c}$ in the rest frame of the B_c meson. Especially for the $B_c \rightarrow D$ decay, the light \bar{u} quark in D meson will typically recoil with the momentum comparable to or larger than the c quark mass due to the large recoil effect for $B_c \rightarrow D$ decay. In order for the final D meson to be bound, there must be a correspondingly large momentum transfer to the spectator c quark. Thus, the overlap between the initial and final meson wave functions at the maximum-recoil point is limited and yields smaller value of $f_+(0)$ for $B_c \rightarrow D$ decay than that for other processes. We also note that one cannot apply the heavy quark symmetry to the system with the two heavy quarks, due to the flavor symmetry breaking by the kinetic energy terms as discussed in [47]. As for the zero-mode contributions, we find that the zero-mode contributions to $f_0(q^2)$ (or $f_-(q^2)$) for the $B_c \rightarrow D, B_c \rightarrow B$ and $B_c \rightarrow B_s$ processes are relatively larger than that for the $B_c \rightarrow \eta_c$ process. For the $B_c \rightarrow \eta_c$ transition, the zero-mode contributions to $f_0(q^2)$ obtained from both linear and HO potential models are almost suppressed in the whole kinematical range and moreover the values of $f_0(q_{\max}^2)$ almost converge to a single value regardless of the choice of potential.

Although there already exist various model predictions on the above B_c semileptonic decays, the predictions of the semileptonic $\eta_b \rightarrow B_c$ decay is not reported yet as far as we know. We thus show in Fig. 8 the q^2 -dependence of the weak form factors $f_+(q^2)$ and $f_0(q^2)$ for the semileptonic $\eta_b \rightarrow B_c$ decay obtained from both linear and HO potential models. The same line codes presented in Fig. 6 are used in Fig. 8. While the linear and HO potential models give similar decay constants for heavy-light mesons (D, B, B_s) and η_c meson [28], they predict quite different values of B_c and η_b , e.g., $f_{\eta_b} = 507$ MeV and

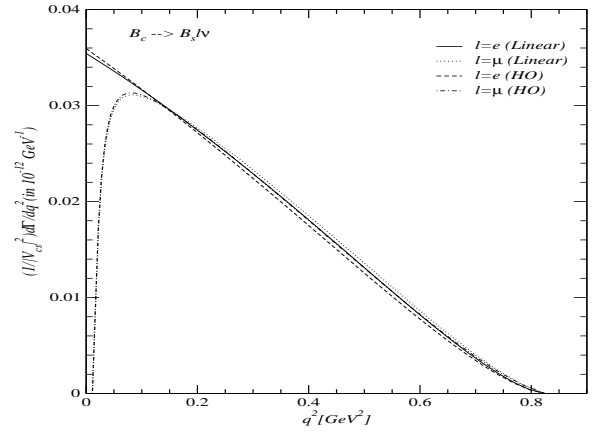
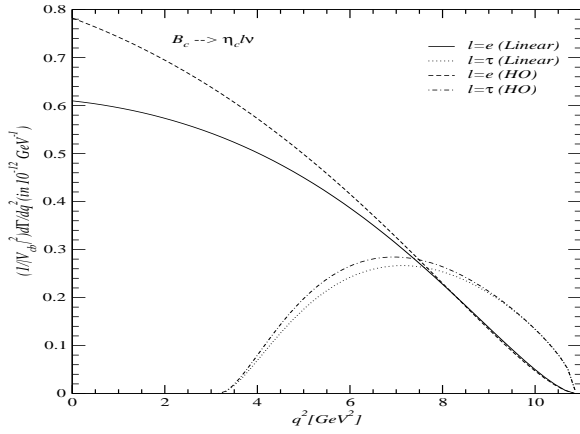
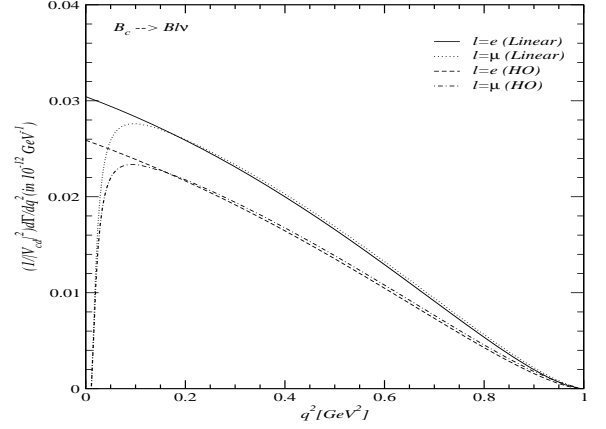
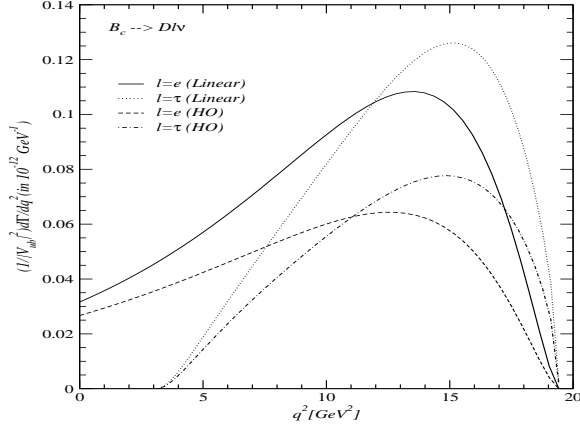


FIG. 9: Differential decay widths $(1/|V_{Q_1 Q_2}|^2)d\Gamma/dq^2$ (in units of $10^{-12} \text{ GeV}^{-1}$) for $B_c \rightarrow D l \nu_\ell$ and $B_c \rightarrow \eta_c l \nu_\ell$ processes obtained from the linear and HO potential parameters.

FIG. 10: Differential decay widths $(1/|V_{Q_1 Q_2}|^2)d\Gamma/dq^2$ (in units of $10^{-12} \text{ GeV}^{-1}$) for $B_c \rightarrow B l \nu_\ell$ and $B_c \rightarrow B_s l \nu_\ell$ processes obtained from the linear and HO potential parameters.

897 MeV for the linear and HO potential models [28], respectively. This results in sizable differences between the two models for the predictions of $f_+(q^2)$ and $f_0(q^2)$ in the $\eta_b \rightarrow B_c$ decay. Since the linear potential model prediction of the quark DA for η_b is narrower than the HO model prediction (see Fig. 4), the overlap between the initial and final meson wave functions at the maximum-recoil point (i.e., $q^2 = 0$) produces smaller values of $f_+(=f_0)$ for the linear potential model than for the HO potential model. The experimental measurement of this process may also distinguish between the linear and HO potential models within our LFQM. The zero-mode contribution to $f_-(q^2)$ (or $f_0(q^2)$) is again quite suppressed in the whole kinematical range as in the case of $B_c \rightarrow \eta_c$ process.

In Figs. 9-11, we show the differential decay widths $d\Gamma/dq^2$ for the $B_c \rightarrow D(\eta_c)l\nu_\ell$ (Fig. 9), $B_c \rightarrow B(B_s)l\nu_\ell$ (Fig. 10) and $\eta_b \rightarrow B_c l\nu_\ell$ (Fig. 11) processes obtained from the linear and HO potential parameters. The line codes are described in each figure. We should note that

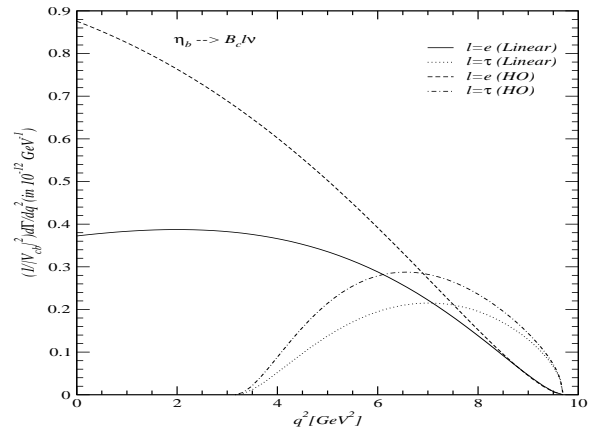


FIG. 11: Differential decay width $(1/|V_{Q_1 Q_2}|^2)d\Gamma/dq^2$ (in units of $10^{-12} \text{ GeV}^{-1}$) for $\eta_b \rightarrow B_c l \nu_\ell$ process obtained from the linear and HO potential parameters.

the minimum q^2 value of the form factor depends on the actual final lepton and it is given (neglecting neutrino masses) by the lepton mass as $q_{\min}^2 = m_\ell^2$. Although the difference between the linear and HO model predictions are not very large for the $B_c \rightarrow (B, B_s)$ processes, they are quite different for other processes, especially for the $\eta_b \rightarrow B_c$ process. Since the constituent masses of b - and c quarks are common to both linear and HO potential models, the difference of the decay rates for the $\eta_b \rightarrow B_c$ process seems to come from the different choice of the variational β parameters. We note, however, that the difference of the decay rates between the two models are significantly reduced for the heavy τ lepton case.

In Table III, we summarize our results for the weak form factors f_+ and f_0 at $q^2 = 0$ and q_{\max}^2 and the decay widths Γ_ℓ of the semileptonic $B_c \rightarrow (D, \eta_c, B, B_s)\ell\nu_\ell$ and $\eta_b \rightarrow B_c\ell\nu_\ell$ ($\ell = e, \mu, \tau$) decays in comparison with other theoretical model predictions [5, 9, 10, 13, 14, 15, 16, 17, 48]. The subscript for the decay width Γ_ℓ represents the result for $P \rightarrow P\ell\nu_\ell$ decay where the final lepton is $\ell = e, \mu$ or τ . For the decays induced by $b \rightarrow u(c)$ transitions such as $B_c \rightarrow D, \eta_c$ and $\eta_b \rightarrow B_c$ decays, we take $\Gamma_e \simeq \Gamma_\mu$ with the massless lepton limit since the muon mass effect is negligible for these transitions with large kinematic ranges. For the decays induced by $c \rightarrow d(s)$ transitions such as $B_c \rightarrow B(B_s)$ decays, Γ_μ is about 5% smaller than Γ_e in our model predictions. For the $B_c \rightarrow D$ decay, our predictions of the form factor f_+ at the maximum-recoil point are rather smaller than other quark model predictions. The upcoming experimental study planned at the Tevatron and at the LHC may distinguish these different model predictions. For the $B_c \rightarrow \eta_c, B$ and B_s semileptonic decays, our predictions are quite comparable with those of the quasipotential approach to the relativistic quark model [9, 10], the relativistic quark-meson model [15], and the nonrelativistic quark model [16]. It may be noted, however, that the predictions of the quark model based on an effective Lagrangian describing the coupling of hadrons to their constituent quarks [5] as well as the covariant LFQM [17] are quite different from other model predictions including ours.

Finally, in order to analyze the total rate for the radiative $B_c^* \rightarrow B_c + \gamma$ decay, the masses of the B_c and B_c^* mesons must be specified. Although we predicted the above two meson masses in Fig. 2, we use the central value of the experimental data $M_{B_c}^{\text{exp}} = 6.276$ GeV [40] to reduce the possible theoretical uncertainties. For the unmeasured B_c^* meson mass, we take some range of the B_c^* meson mass, i.e., $10 \text{ MeV} \leq \Delta m (= M_{B_c^*} - M_{B_c}) \leq 220 \text{ MeV}$. The upper value of Δm (i.e., $M_{B_c^*} = 6496$ MeV) is chosen to be corresponding to our predictions, $M_{B_c^*} = 6494$ MeV and 6492 MeV, obtained from the linear and HO potential models, respectively.

In Fig. 12, we show the momentum-dependent form factor $F_{B_c^*B_c}(q^2)$ (upper panel) for the radiative $B_c^* \rightarrow B_c\gamma^*$ decay and the dependence of $\Gamma(B_c^* \rightarrow B_c\gamma)$ on Δm (lower panel) obtained from the linear (solid line) and

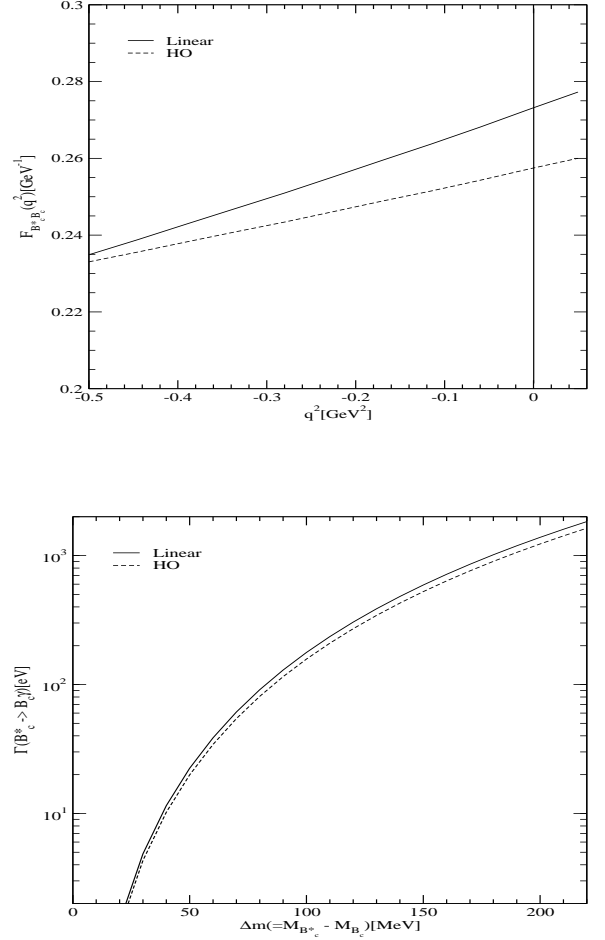


FIG. 12: The transition form factor $F_{B_c^*B_c}(q^2)$ (upper panel) for $B_c^* \rightarrow B_c\gamma^*$ and the dependence of $\Gamma(B_c^* \rightarrow B_c\gamma)$ (lower panel) on $\Delta m = M_{B_c^*} - M_{B_c}$ obtained from the linear and HO potential parameters, where the central value of the experimental data $M_{B_c}^{\text{exp}} = 6.276$ GeV [40] is used.

HO potential (dashed line) parameters. For the transition form factor $F_{B_c^*B_c}(q^2)$, we have performed the analytic continuation of $F_{B_c^*B_c}(q^2)$ from the spacelike region ($q^2 < 0$) to the physical timelike $0 \leq q^2 \leq q_{\max}^2$, where $q_{\max}^2 = (M_{B_c^*} - M_{B_c})^2$ represents the zero recoil point of the B_c meson. The coupling constant $g_{B_c^*B_c}$ is obtained at the $q^2 = 0$ point that corresponds to the B_c meson recoiling with the maximum three-momentum in the rest frame of the B_c^* meson. In our model calculation, the coupling constant itself is independent of the physical masses of the mesons and our prediction is $g_{B_c^*B_c} = 0.273$ [0.257] GeV^{-1} for the linear [HO] potential model. Our predictions are quite comparable with the result from the QCD sum rule approach [49], $g_{B_c^*B_c}^{SR} = 0.270 \pm 0.095$ GeV^{-1} . As one can see from the lower panel of Fig. 12, the dependence of $\Gamma(B_c^* \rightarrow B_c\gamma)$ on Δm is quite sensitive to the mass of the B_c^* meson, e.g., our linear [HO] poten-

TABLE III: Form factors f_+ and f_0 evaluated at $q^2 = 0$ and q_{max}^2 and decay widths Γ_ℓ (in 10^{-15} GeV) for $B_c \rightarrow (D, \eta_c, B, B_s)\ell\nu_\ell$ and $\eta_b \rightarrow B_c\ell\nu_\ell$ ($\ell = e, \mu, \tau$) transitions.

Mode	Linear[HO]	EFG [9, 10]	IKS [5]	NW [15]	HNV [16]	AKN [48]	CD [14]	WSL [17]	
$B_c \rightarrow D$	$f_{+(0)}(0)$	0.086[0.079]	0.14	0.69	0.1446	-	0.089	0.16	
	$f_+(q_{\text{max}}^2)$	1.129[0.789]	1.20	2.20	1.017	-	0.59	1.10	
	$f_0(q_{\text{max}}^2)$	0.673[0.554]	0.64	-	-	-	-	0.59	
	$\Gamma_{e(\mu)}$	0.021[0.014]	0.019	0.26	0.020	-	-	0.005(0.03)	0.043
	Γ_τ	0.019[0.012]	-	-	-	-	-	-	-
$B_c \rightarrow \eta_c$	$f_{+(0)}(0)$	0.482[0.546]	0.47	0.76	0.5359	0.49	0.622	0.61	
	$f_+(q_{\text{max}}^2)$	1.084[1.035]	1.07	1.07	1.034	1.00	-	0.94	1.10
	$f_0(q_{\text{max}}^2)$	0.876[0.872]	0.92	-	-	0.91	-	-	0.86
	$\Gamma_{e(\mu)}$	6.93[7.95]	5.9	14.0	6.8	6.95	8.6	2.1(6.9)	9.81
	Γ_τ	2.31[2.46]	-	3.52	-	2.46	3.3 ± 0.9	-	-
$B_c \rightarrow B$	$f_{+(0)}(0)$	0.464[0.428]	0.39	0.58	0.4504	0.39	0.362	0.63	
	$f_+(q_{\text{max}}^2)$	0.729[0.647]	0.96	0.96	0.6816	0.70	-	0.66	0.97
	$f_0(q_{\text{max}}^2)$	0.572[0.570]	0.80	-	-	0.71	-	-	0.81
	Γ_e	0.84[0.69]	0.6	2.1	0.638	0.65	-	0.9(1.0)	1.63
	Γ_μ	0.80[0.67]	-	-	-	0.63	-	-	-
$B_c \rightarrow B_s$	$f_{+(0)}(0)$	0.570[0.574]	0.50	0.61	0.5917	0.58	0.564	0.73	
	$f_+(q_{\text{max}}^2)$	0.802[0.771]	0.99	0.92	0.8075	0.86	-	0.66	1.03
	$f_0(q_{\text{max}}^2)$	0.685[0.716]	0.86	-	-	0.86	-	-	0.87
	Γ_e	15.45[15.20]	12	29	12.35	15.1	15	11.1(12.9)	23.45
	Γ_μ	14.61[14.40]	-	-	-	14.5	-	-	-
$\eta_b \rightarrow B_c$	$f_{+(0)}(0)$	0.341[0.523]	-	-	-	-	-	-	
	$f_+(q_{\text{max}}^2)$	0.976[0.918]	-	-	-	-	-	-	
	$f_0(q_{\text{max}}^2)$	0.811[0.839]	-	-	-	-	-	-	
	$\Gamma_{e(\mu)}$	4.64[7.94]	-	-	-	-	-	-	
	Γ_τ	1.57[2.11]	-	-	-	-	-	-	

tial model predicts $\Gamma(B_c^* \rightarrow B_c\gamma) = 22.4$ [19.9] eV \sim 1836 [1631] eV for $\Delta m = 50$ MeV \sim 220 MeV. This sensitivity for the B_c^* radiative decay may help in determining the mass of B_c^* experimentally and pinning down the best phenomenological model. Other magnetic dipole decays $V \rightarrow P\gamma$ of various heavy-flavored mesons such as $(D, D^*, D_s, D_s^*, \eta_c, J/\psi)$ and $(B, B^*, B_s, B_s^*, \eta_b, \Upsilon)$ using our LFQM can be found in [28].

VII. SUMMARY AND DISCUSSION

In this work, we investigated the exclusive semileptonic $B_c \rightarrow (D, \eta_c, B, B_s)\ell\nu_\ell$, $\eta_b \rightarrow B_c\ell\nu_\ell$ ($\ell = e, \mu, \tau$) decays and the magnetic dipole $B_c^* \rightarrow B_c\gamma$ decay using our LFQM constrained by the variational principle for the QCD motivated effective Hamiltonian with the linear (or HO) plus Coulomb interaction. Especially, we obtained the new variational parameter β_{cb} for the bottom-charm sector and predicted the mass eigenvalues of the low-lying B_c and B_c^* states. Our new predictions of $M_{B_c} = 6459$ [6351] MeV obtained from the linear [HO] potential model is in agreement with the data, $M_{B_c}^{\text{exp}} = (6276 \pm 4)$ MeV [40], within 3% error. We also predicted the unmeasured mass of B_c^* as $M_{B_c^*} = 6494$ [6496] MeV for the linear [HO] potential model. Our model parameters obtained from the variational principle uniquely determine the physical quantities related to the above processes. This approach can establish the broader applicability of

our LFQM to the wider range of hadronic phenomena. For instance, our LFQM has been tested extensively in the spacelike processes [24, 50] as well as in the timelike exclusive processes such as semileptonic [25, 26, 32] and rare [27] decays of pseudoscalar mesons and the magnetic dipole $V \rightarrow P\gamma^*$ decays [28, 29].

The weak form factor $f_\pm(q^2)$ for the semileptonic decays between two pseudoscalar mesons and the decay form factor $F_{B_c^* B_c}(q^2)$ for the $B_c^* \rightarrow B_c\gamma$ decay are obtained in the $q^+ = 0$ frame ($q^2 = -\mathbf{q}_\perp^2 < 0$) and then analytically continued to the timelike region by changing \mathbf{q}_\perp^2 to $-q^2$ in the form factor. The covariance (i.e., frame independence) of our model has been checked by performing the LF calculation in the $q^+ = 0$ frame in parallel with the manifestly covariant calculation using the exactly solvable covariant fermion field theory model in $(3+1)$ -dimensions. We found the zero-mode contribution to the form factor $f_-(q^2)$ and identified the zero-mode operator that is convoluted with the initial and final state LF wave functions. We calculated the decay constants of (B_c, B_c^*) mesons and the decay rates for the exclusive $B_c \rightarrow (D, \eta_c, B, B_s)\ell\nu_\ell$ and $\eta_b \rightarrow B_c\ell\nu_\ell$ decays and compared with other theoretical approaches. Particularly, the decay constants for (B_c, B_c^*) mesons and the decay rate for $\eta_b \rightarrow B_c$ process are quite sensitive to the choice of potential within our LFQM. From the future experimental data on these sensitive processes, one may obtain more realistic information on the potential between quark and antiquark in the heavy meson sys-

tem.

For the radiative $B_c^* \rightarrow B_c \gamma$ decay, we find that the decay width $\Gamma(B_c^* \rightarrow B_c \gamma)$ is very sensitive to the value of $\Delta m = M_{B_c^*} - M_{B_c}$. This sensitivity for the B_c^* radiative decay may help in determining the mass of B_c^* experimentally. Since the form factor $F_{B_c^* B_c}(q^2)$ for the radiative $B_c^* \rightarrow B_c \gamma$ decay presented in this work is analogous to the vector current form factor $g(q^2)$ in the weak decay of ground state vector meson to ground state pseudoscalar meson, the ability of our model in describing the radiative decay would therefore be relevant to the applicability of our model also for the weak decay. Consideration on

such exclusive weak decays in our LFQM is underway.

Acknowledgments

The work of H.-M. Choi was supported by the Korea Research Foundation Grant funded by the Korean Government(KRF-2008-521-C00077) and that of C.-R. Ji by the U.S. Department of Energy(No. DE-FG02-03ER41260).

-
- [1] I. P. Gouz, V. V. Kiselev, A. K. Likhoded, V. I. Romanovsky, and O. P. Yushchenko, *Phys. Atom. Nucl.* **67**, 1559 (2004); *Yad. Fiz.* **67**, 1581 (2004).
- [2] P. Colangelo, G. Nardulli, and N. Paver, *Z. Phys. C* **57**, 43 (1993).
- [3] V. V. Kiselev, A. E. Kovalsky, and A. K. Likhoded, *Nucl. Phys. B* **585**, 353 (2000); V. V. Kiselev, A. K. Likhoded, and A. I. Onishchenko, *Nucl. Phys. B* **569**, 473 (2000).
- [4] T. Huang and F. Zuo, *Eur. Phys. J. C* **51**, 833 (2007).
- [5] M. A. Ivanov, J. G. Körner and P. Santorelli, *Phys. Rev. D* **63**, 074010 (2001).
- [6] M. A. Ivanov, J. G. Körner and P. Santorelli, *Phys. Rev. D* **71**, 094006 (2005).
- [7] M. A. Ivanov, J. G. Körner and P. Santorelli, *Phys. Rev. D* **73**, 054024 (2006).
- [8] D. Ebert, R. N. Faustov and V. O. Galkin, *Phys. Rev. D* **67**, 014027 (2003).
- [9] D. Ebert, R. N. Faustov and V. O. Galkin, *Phys. Rev. D* **68**, 094020 (2003).
- [10] D. Ebert, R. N. Faustov and V. O. Galkin, *Eur. Phys. J. C* **32**, 29 (2003).
- [11] C.-H. Chang and Y.-Q. Chen, *Phys. Rev. D* **49**, 3399 (1994).
- [12] J.-F. Liu and K.-T. Chao, *Phys. Rev. D* **56**, 4133 (1997).
- [13] A. Abd El-Hady, J. H. Munoz, and J. P. Vary, *Phys. Rev. D* **62**, 014019 (2000).
- [14] P. Colangelo and F. De Fazio, *Phys. Rev. D* **61**, 034012 (2000).
- [15] M. A. Nobes and R. M. Woloshyn, *J. Phys. G* **26**, 1079 (2000).
- [16] E. Hernández, J. Nieves and J. M. Verde-Velasco, *Phys. Rev. D* **74**, 074008 (2006).
- [17] W. Wang, Y.-L. Shen, and C.-D. Lü, arXiv:0811.3748[hep-ph].
- [18] M. Lusignoli and M. Masetti, *Z. Phys. C* **51**, 549 (1991).
- [19] D. Du and Z. Wang, *Phys. Rev. D* **39**, 1342 (1989).
- [20] R. Dhir, N. Sharma, and R.C. Verma, *J. Phys. G* **35**, 085002 (2008).
- [21] S. Godfrey, *Phys. Rev. D* **70**, 054017 (2004).
- [22] M. Wirbel, B. Stech, and M. Bauer, *Z. Phys. C* **29**, 637 (1985); M. Bauer, B. Stech, and M. Wirbel, *Z. Phys. C* **34**, 103 (1987).
- [23] N. Isgur, D. Scora, B. Grinstein, and M.B. Wise, *Phys. Rev. D* **39**, 799 (1989).
- [24] H.-M. Choi and C.-R. Ji, *Phys. Rev. D* **59**, 074015 (1999).
- [25] H.-M. Choi and C.-R. Ji, *Phys. Lett. B* **460**, 461 (1999).
- [26] C.-R. Ji and H.-M. Choi, *Phys. Lett. B* **513**, 330 (2001).
- [27] H.-M. Choi, C.-R. Ji, and L.S. Kisslinger, *Phys. Rev. D* **65**, 074032 (2002).
- [28] H.-M. Choi, *Phys. Rev. D* **75**, 073016 (2007); *J. Korean Phys. Soc.* **53**, 1205 (2008).
- [29] H.-M. Choi, *Phys. Rev. D* **77**, 097301 (2008).
- [30] H.-M. Choi and C.-R. Ji, *Phys. Rev. D* **58**, 071901(R) (1998); *Phys. Rev. D* **72**, 013004 (2005); S. J. Brodsky and D. S. Hwang, *Nucl. Phys. B* **543**, 239 (1998); M. Burkardt, *Phys. Rev. D* **47**, 4628 (1993); J.P.B.C. de Melo, J.H.O. Sales, T. Frederico, and P.U. Sauer, *Nucl. Phys. A* **631**, 574 (1998c).
- [31] W. Jaus, *Phys. Rev. D* **60**, 054026 (1999).
- [32] H.-M. Choi and C.-R. Ji, *Phys. Rev. D* **59**, 034001 (1998).
- [33] B.L.G. Bakker, H.-M. Choi, and C.-R. Ji, *Phys. Rev. D* **63**, 074014 (2001).
- [34] B.L.G. Bakker, H.-M. Choi, and C.-R. Ji, *Phys. Rev. D* **67**, 113007 (2003).
- [35] J.P.B.C. de Melo and T. Frederico, *Phys. Rev. C* **55**, 2043 (1997); J.P.B.C. de Melo, T. Frederico, E. Pace, and G. Salme, *Phys. Rev. D* **73**, 074013 (2006).
- [36] J. Carbonell, B. Desplanques, V.A. Karmanov, and J.-F. Mathiot, *Phys. Rep.* **300**, 215 (1998).
- [37] A. Szczepaniak, C.-R. Ji, and S.R. Cotanch, *Phys. Rev. D* **52**, 5284 (1995).
- [38] H.-M. Choi and C.-R. Ji, *Phys. Rev. D* **75**, 034019 (2007).
- [39] D. Scora and N. Isgur, *Phys. Rev. D* **52**, 2783 (1995).
- [40] C. Amsler *et al.* (Particle Data Group), *Phys. Lett. B* **667**, 1 (2008).
- [41] P. Grenier, arXiv:0809.1672 [hep-ex].
- [42] E. J. Eichten and C. Quigg, *Phys. Rev. D* **49**, 5845 (1994).
- [43] S. S. Gershtein, V. V. Kiselev, A. K. Likhoded, and A.V. Tkabladze, *Phys. Rev. D* **51**, 3613 (1995).
- [44] L. P. Fulcher, *Phys. Rev. D* **60**, 074006 (1999).
- [45] S. Capstick and S. Godfrey, *Phys. Rev. D* **41**, 2856 (1990).
- [46] G. P. Lepage and S. J. Brodsky, *Phys. Rev. D* **22**, 2157 (1980).
- [47] E. Jenkins, M. Luke, A. V. Manohar, and M. J. Savage, *Nucl. Phys. B* **390**, 463 (1993).
- [48] A.Yu. Anisimov, P. Yu. Kulikov, I.M. Narodetskii, and K.A. Ter-Martirosyan, *Phys. Atom Nucl.* **62**, 1739 (1999)[*Yad. Fiz.* **62**, 1868 (1999)].
- [49] T. M. Aliev, E. Iltan, and N. K. Pak, *Phys. Lett. B* **329**, 123 (1994).

- [50] H.-M. Choi, C.-R. Ji, and L.S. Kisslinger, Phys. Rev. D **64**, 093006 (2001); Phys. Rev. D **66**, 053011 (2002).